UNIVERSITÀ DEGLI STUDI DI GENOVA

SCUOLA POLITECNICA

DIME

Dipartimento di Ingegneria Meccanica, Energetica, Gestionale e dei Trasporti

TESI DI LAUREA MAGISTRALE IN
INGEGNERIA MECCANICA – ENERGIA E AERONAUTICA

Progettazione e Modellazione di un ciclo supercritico a circuito chiuso per l'Impianto VLF

Relatori:

Chiar.mo Prof. Ing. Guglielmo Lomonaco

Dr. Ing. Marco Caramello

Candidato:

Andrea Ortona

Dicembre 2025

<< *I piedi miei non toccan più*
Sto volando dentro il blu
E' strano e bello guardar da qui
E veder le case piccole così
Il mondo cambia da quassù
Non ha barriere più
E tutto questo, amici miei
Io lo devo solo a voi >>

(*So Volare*, Ivana Spagna, 1998)

Design and modeling of a closed-loop supercritical cycle for the VLF facility

Abstract

In the present thesis is going to be studied the closure of the secondary loop of the Versatile Loop Facility, an experimental facility cycle, whose purpose is testing the main components of the IV generation Lead Fast Reactors. Heat removal from the primary lead loop is managed by a supercritical water-cooling open loop, so the first chapter faces the study of supercritical water as coolant, going deeper in its features. Then, a description of the actual secondary open design of the VLF is presented. After this, the system code RELAP5 and the loop nodalization used for the thermal-hydraulic transient is described. In the fourth chapter different concept designs of possible solutions for the closed cycle are studied, facing pros and cons of each one. In the end, verifying the stability on the closed cycle, a possible incidental transient analysis of the final closed loop design is shown, working on an existing RELAP5 model.

Progettazione e Modellazione di un ciclo supercritico a circuito chiuso per l'Impianto VLF

Sommario

Nella presente tesi verrà studiata la chiusura del circuito secondario dell'impianto Versatile Loop Facility, un ciclo sperimentale il cui scopo è testare i componenti principali dei reattori veloci al piombo di quarta generazione. La rimozione del calore dal circuito primario in piombo è gestita da un circuito aperto di raffreddamento ad acqua supercritica, pertanto il primo capitolo affronta lo studio dell'acqua supercritica come refrigerante, approfondendone le caratteristiche. Successivamente, viene presentata una descrizione dell'attuale design aperto del secondario del VLF. Dopodiché, vengono descritti il codice di sistema RELAP5 e la nodalizzazione del circuito utilizzata per il transitorio termoidraulico. Nel quarto capitolo vengono studiati diversi progetti concettuali di possibili soluzioni per il ciclo chiuso, affrontando i pro e i contro di ciascuno. Infine, verificando la stabilità del ciclo chiuso, viene mostrata una possibile analisi transitoria incidentale del progetto finale del circuito chiuso, lavorando su un modello RELAP5 esistente.

Summary

1. Introduction

1.1 International energy context

The international energy context is marked by significant changes related to the transition to sustainable sources, supply security and geopolitical dynamics. The growing global demand, especially from emerging economies, clashes with the need to reduce greenhouse gas emissions, because the most economical energy sources are, typically, the most polluting, like coal. So, it is needed to accelerate the development of renewable energy and green technologies. At the same time, political tensions in strategic areas, such as the Middle East or Easter Europe, affect market stability, making source diversification and energy independence key priorities for many countries [1].
In this perspective, innovative nuclear reactors are needed mainly for their more efficient fuel use, lower emissions, better waste management and improvement in passive safety compared to previous generations. Also, the flexibility of new applications such as Small Modular Reactors (SMR) and the possibility of a series production, reducing times and costs, improve the economic competitiveness.

1.2 Generation IV reactors and LFR

Fourth generation nuclear reactor represent the future of nuclear energy, aiming to improve safety, efficiency and sustainability compared to previous designs. These advanced reactors are designed to minimize waste, operate at higher temperatures and in some cases recycle spent fuel. Many of them incorporate passive safety system that reduce the risk of accidents. Currently under research and development, IV-Gen technologies are expected to play a key role in the global transition to low carbon energy over the coming decades. One of the most promising designs is the Lead Fast Reactor, a reactor that uses liquid lead or lead-bismuth eutectic as coolant. These reactors operate at high temperatures and use fast neutron spectrum to sustain the nuclear fission chain reaction. LFRs offer several advantages, including enhanced safety due to the high boiling point and inert nature of lead, as well as improved fuel efficiency and waste reduction through closed fuel cycles.
At present, the main LFR demonstrators are the Westinghouse LFR and ALFRED (Advanced LFR European Demonstrator). The first one is a mid-size, highly simplified and passively safe compact reactor plant. Starting from a scalable design architecture, the LFR's has a net power output of 450 MW_e. The plant operates with a fast neutron spectrum core in a pool configuration reactor, which is interfaced with a supercritical CO_2 power conversion system that uses air as the ultimate heat sink.
The ALFRED primary system configuration is pool-type with all components inside removable. It has a simple flow path of the primary coolant, allowing natural circulation. The primary coolant, from the core moves upward through the primary pump and then, through the steam generator, flows down in the cold plenum, reaching the inlet of the core.
In this work an LFR with supercritical water secondary circuit as cooler is presented.

1.3 Supercritical water technology

A supercritical water-cooling system is a water-cooled circuit concept operating at supercritical pressures. When water is pressurized above its thermodynamic critical point of 221 bar, there is not a well-defined distinction between liquid and gas phase. In a general SCWR (supercritical water-cooled reactor) core, reactor coolant water is at low temperature, high density at the inlet, and it becomes high temperature, low density fluid at the outlet, which makes it attractive for a once-through reactor having a direct thermodynamic cycle. The use of supercritical pressure water as coolant reaching high temperatures, enables achieving higher thermal efficiency (up to 48%) and implementing efficient heat transport system configuration. A typical SCW system is designed to operate at the pressure above 250 bar, with average outlet coolant temperature in the range of 500−625 °C depending on the concepts [2]. Figure 1.1 compares pressure and temperature ranges in a typical SCWR with conventional WCRs. For the SCWR, the pressure vessel (PV) and pressure tubes (PT) types are presented.

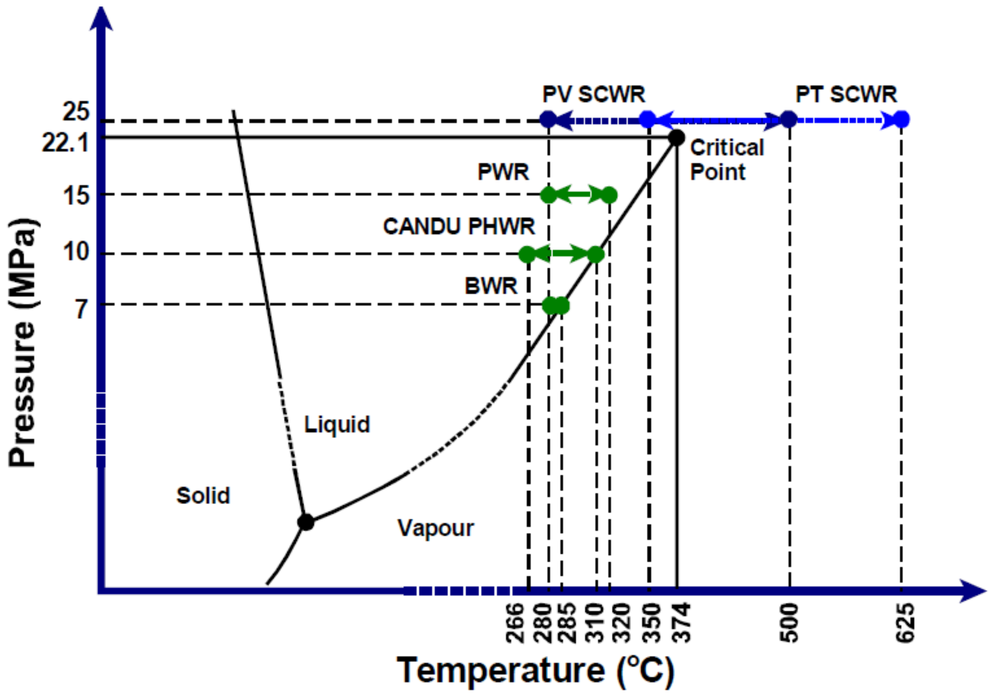

Fig 1.1 – Comparison of pressures and temperatures in water reactors

1.4 Purpose

The purpose of this thesis is designing and modeling a supercritical thermodynamic closed cycle for the Versatile Facility Loop. The work consists of a review of the scientific literature about supercritical cycles, the thermohydraulic and process cycle design, optimizing available components. Finally, dynamic modelling of the system with code RELAP5 is presented, with the aim of verifying operational feasibility through pre-test simulations.

2. Supercritical Water Features

Mainly because of rapid changes in thermo-physical properties across the pseudocritical temperature range and no strict distinction between liquid and gas phases, thermal hydraulic behavior of supercritical water can be very different from subcritical one. For example, near the pseudocritical point there's an enhancement in heat transfer like boiling, but forward there is a degradation typical of high void fraction condition. The substantial difference is in the instantaneous of this changing.

2.1 Introduction

At critical and supercritical pressures, a fluid is considered to be in a single phase, and all thermophysical properties meet significant changes through the critical and pseudocritical regions [3]. Near the critical point, these changes are very important: raising the temperature of water from 350 to 380 °C at the critical pressure of 221 bar, density drops of -72,8%, thermal conductivity drops of -59,4%, dynamic viscosity of -60,4%, the specific heat raises of +172%, while the Prandtl number raises of +165%. Near the pseudocritical point, with an increase in pressure, these changes become less pronounced: for example, with the same temperatures as the previews case, but at 400 bar, density drops of only -11,5%, thermal conductivity drops of -13%, dynamic viscosity of -12,9%, the specific heat raises of +21%, while the Prandtl number raises of +21,1%.
Density and *dynamic viscosity* undergo a significant drop within a very strict temperature range, as we can see in Figure 2.1 and 2.3.
Kinematic viscosity and *specific enthalpy* undergo a sharp increase.
Thermal conductivity, *specific heat*, *Prandtl number* and *volume expansivity* show local peaks near the critical and pseudocritical points, Figures 2.2, 2.4, 2.5.
Thermal conductivity, *dynamic viscosity* and *kinematic viscosity* face their minimum right after the critical and pseudocritical points.
The *specific heat* of water has a maximum value at the critical point. The exact temperature corresponding to the specific heat peak above the critical pressure is known as the pseudocritical temperature.
Figure 2.1 to Figure 2.5 show the properties at the critical (P_{cr} = 22.064 MPa) and four supercritical pressures (P = 25, 30, 35, 40 MPa). Figure 2.7 shows selected thermophysical properties near the pseudocritical point of water at 25 MPa.

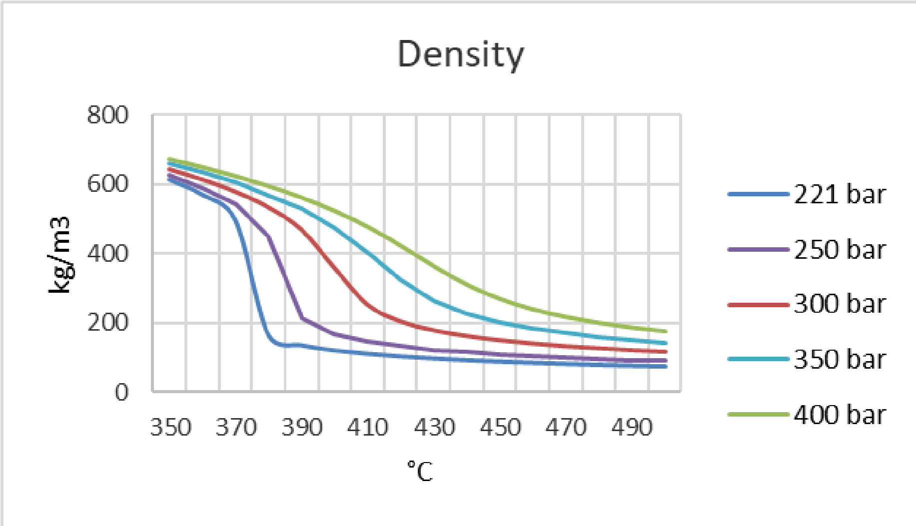

Fig. 2.1 - Variations of water density with temperature.

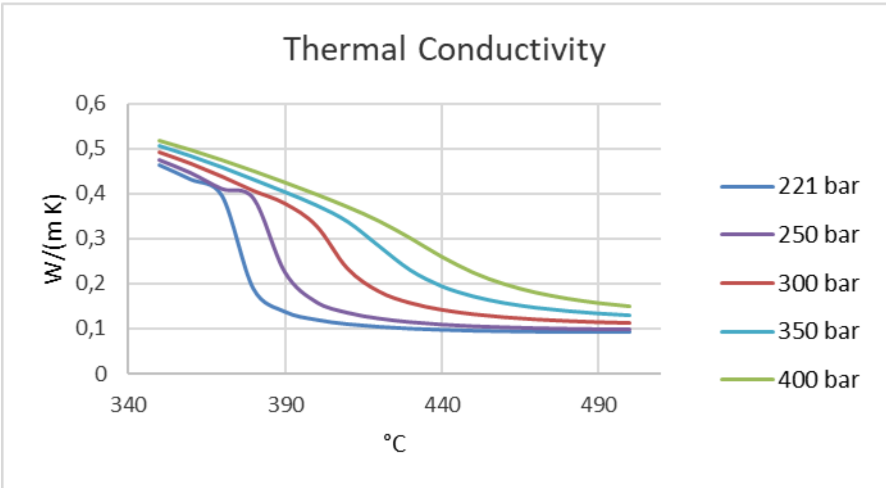

Fig. 2.2 - Variations of water thermal conductivity with temperature.

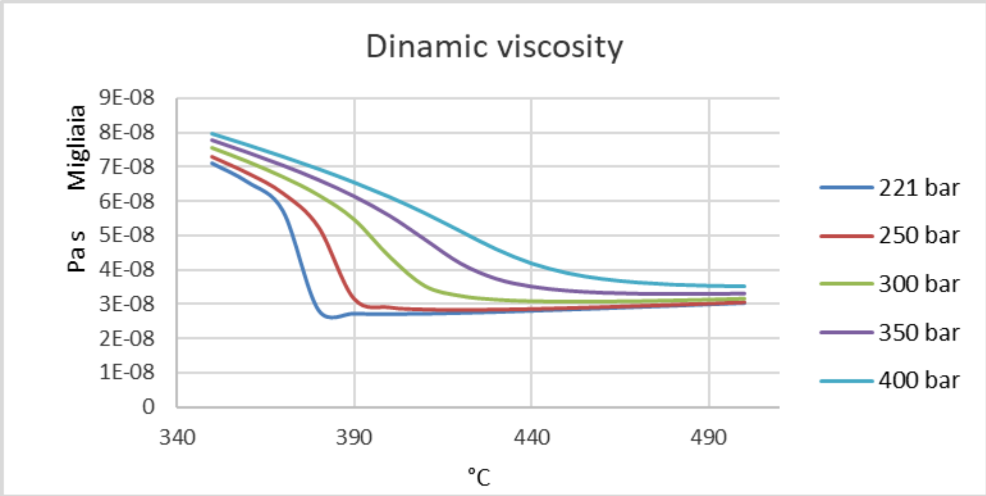

Fig. 2.3 - Variations of water dynamic viscosity with temperature.

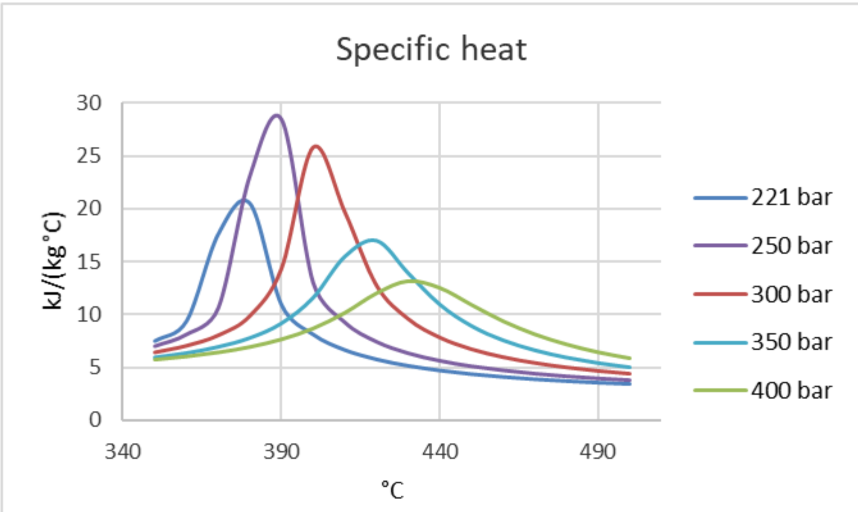

Fig. 2.4 - Variations of water specific heat at constant pressure with temperature.

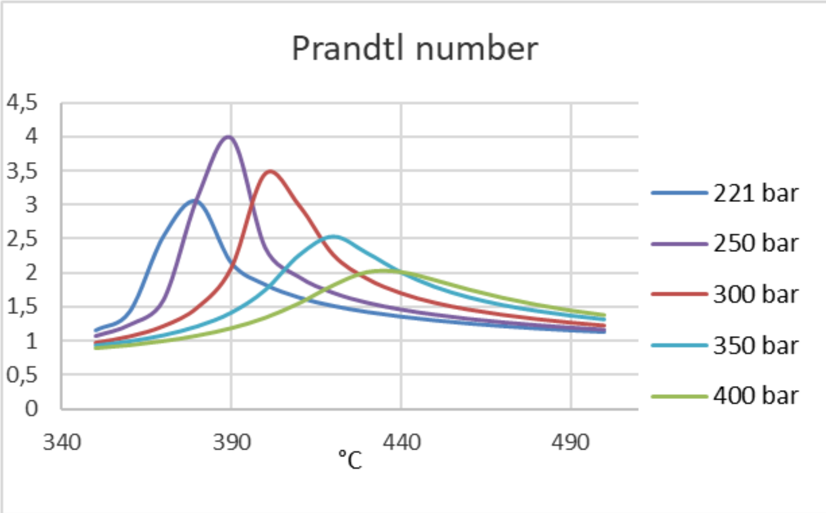

Fig. 2.5 - Variations of water Prandtl number with temperature.

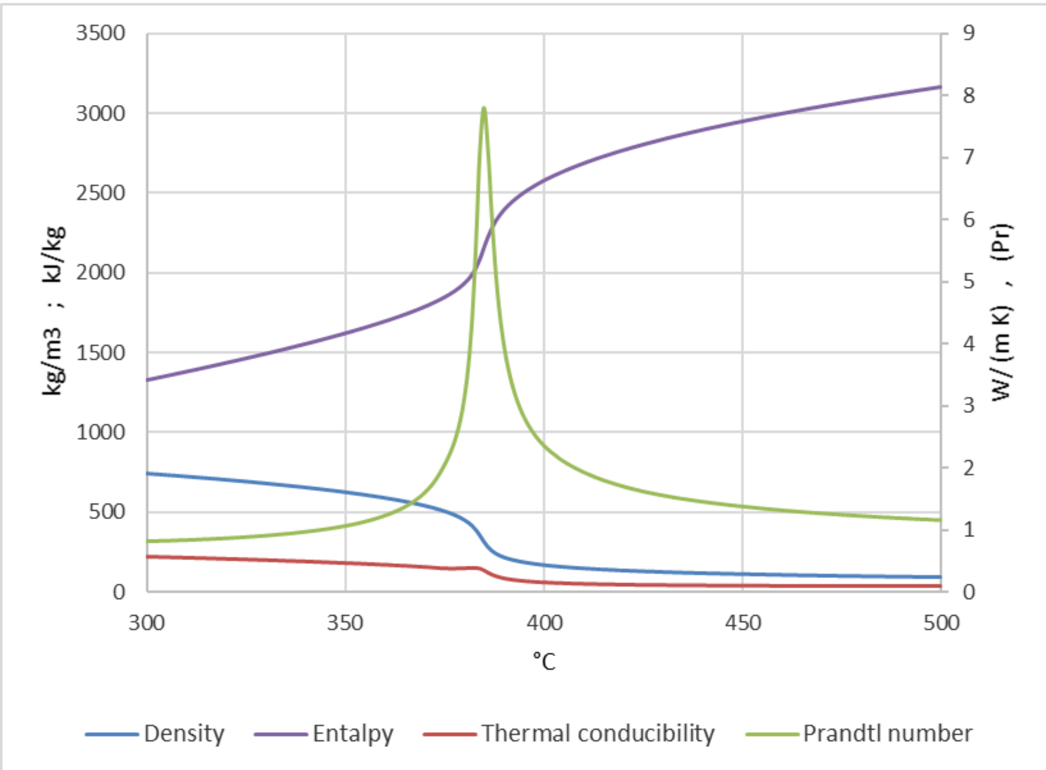

Fig. 2.6 - Variations of selected thermophysical properties of water in pseudocritical region (around the pseudocritical point of 384.9°C).

In Figure 2.8 we can see the same parameters of Figure 2.7 but in the range temperature of a classic core of a PWR, so we can appreciate their different behaviors. The trend is quite uniform, but at 342 °C, density and thermal conductivity suddenly drop, while Prandtl number and enthalpy rise. The Prandtl number is the most varying parameter from one case to another, quite doubling its value in the PWR case but presenting a cusp in the SCW.

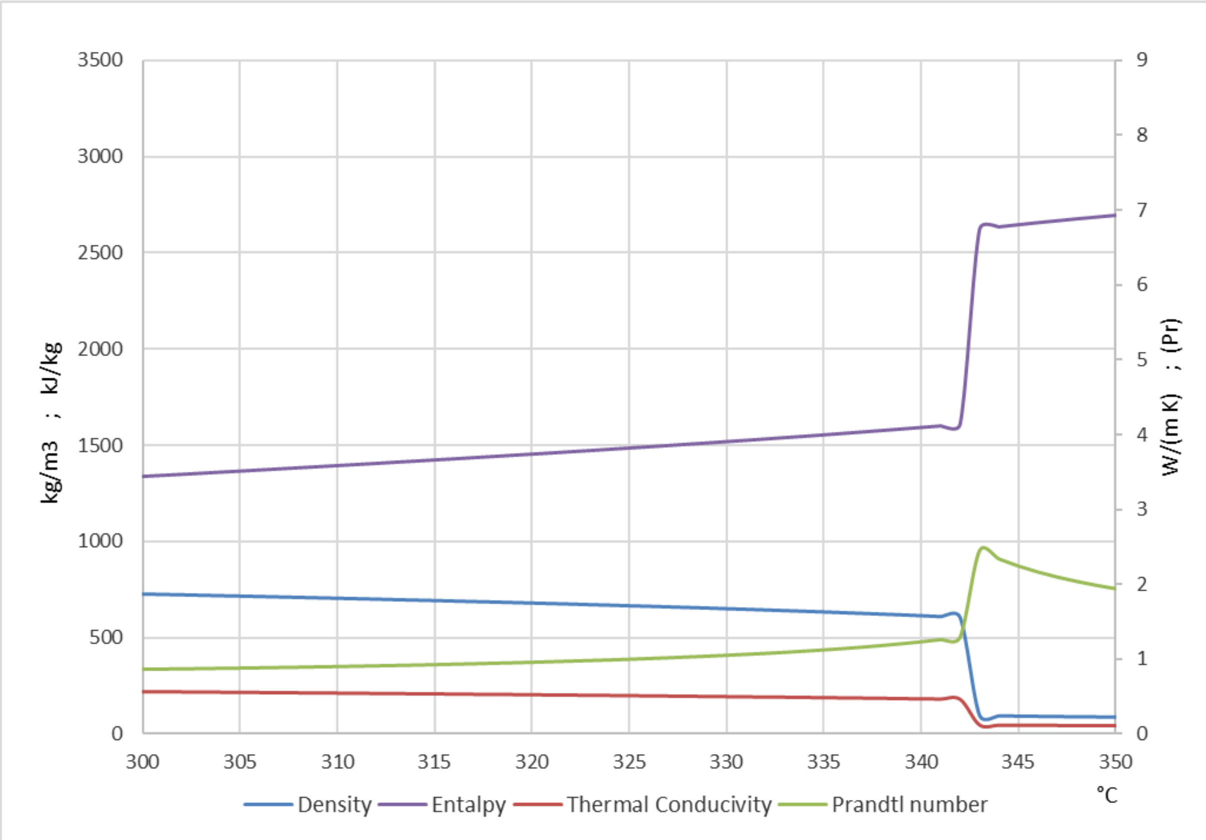

Fig. 2.7 - Variations of selected thermophysical properties of water at 150 bar.

2.2 Thermal Hydraulics

2.2.1 SCW heat transfer correlations

The heat transfer in supercritical water flow is a complex phenomenon caused by the nonlinear variations of thermophysical properties in turbulent flows at different thermal load conditions [4]. Most of the correlation published in the literature for heat transfer to water, even under supercritical pressure conditions, comes from experimental studies results rather than computational evaluations using turbulence models. Test conditions and parametric ranges for applications vary considerably. Most correlations have the form of the Dittus-Boelter equation with some modifications [5]. The most commonly used dimensionless parameters in the correlation equations are Nu, Re, Pr, Gr and nondimensional fluid property ratios. The first correlation was proposed by McAdams [6] for heat transfer in SCW flow and was based on the Dittus–Boelter correlation [7], formula (2.1),

$$Nu_b = 0.023 Re_b^{0.8} Pr_b^{0.4} \tag{2.1}$$

Where

$$Nu_b = \frac{h\,D}{k_b}$$

$$Re_b = \frac{G\,D}{\mu_b}$$

$$Pr_b = \frac{c_{p,b}\,\mu_b}{k_b}$$

This correlation agrees with experimental data obtained with SCW flow in circular tubes at different pressures and low thermal loads [8], but valuates unrealistically the heat transfer in case of deteriorated heat transfer (DHT), near the critical and pseudocritical points. The issue was attributed to its strong sensitivity on the variation of thermophysical properties. Many correlations were proposed after the introduction of the McAdams correlation and were expressed in a general form as [9], formula (2.2):

$$Nu_{t,x} = C_1 Re_{t,x}^{m_1} Pr_{t,x}^{m_2} \left(\frac{\rho_t}{\rho_t}\right)_x^{m_3} \left(\frac{\mu_t}{\mu_t}\right)_x^{m_4} \left(\frac{\lambda_t}{\lambda_t}\right)_x^{m_5} \left(1 + C_2 \frac{D_{hy}}{L_h}\right)^{m_7} \tag{2.2}$$

Where *x* represents the axial coordinate, *t* is for turbulent flow and C_1, C_2 are constants.
Many details were related to the review of correlations for SCW flow: we get better results using an averaged isobaric specific heat ($\bar{c}_p$), or using the ratios of thermophysical properties. On one side, the extensive comparisons on these different correlations have exposed that most of them are able to provide usable preliminary estimations for heat transfer of SCW flow in tube and bundle geometries [9], [10], [11]. On the other side, none of the published correlations is capable to predict accurately the DHT cases of SCW flow.

2.2.2 Effect of flow direction

The flow direction of the supercritical coolant can be upward, downward, or both. While most experimental data have been obtained with upward flow in tubes, different experiments examine the heat-transfer characteristics with downward flow. Figure 2.9 compares wall-temperature measurements with upward and downward flows in a 4.4 mm tube. Wall-temperature measurements are lower for downward flow than upward flow, but the difference decrease with increasing bulk-fluid enthalpy. One difference is the absence of a deteriorated heat-transfer conditions with downward flow in the low enthalpy region.

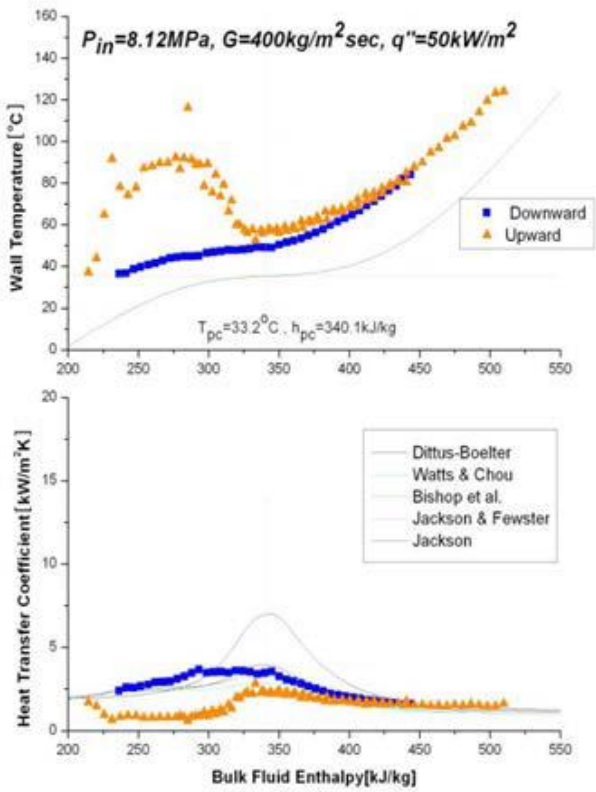

Fig. 2.9 - Effect of flow direction on supercritical heat transfer in tubes.

2.2.3. Overview of past experimental works on heat transfer of SCW flow in tubes

Based on the experimental investigation, different classifications of heat transfer types for SCW were elaborated. The following experimental approach has been used [9]: the geometry of investigated test sections was fixed and all parameters were kept constant except the bulk fluid enthalpy. Then, steady state data were recorded in a selected range of the varying parameter. At the evaluation stage, wall and bulk fluid temperatures were shown as a function of the bulk specific fluid enthalpy (h_b), which is more appropriate than the axial position or the heated length in indicating the pseudocritical enthalpy, h_{pc}, defined as the fluid enthalpy at the supercritical state, when its temperature is the pseudocritical temperature.

Three different heat transfer types and a regeneration of heat transfer phenomenon (OHTR–onset of heat transfer regeneration) were identified from the experimental observations of flow in tubes [4]: the normal heat transfer (NHT), the enhanced heat transfer (EHT), and deteriorated heat transfer (DHT).

These four types of heat transfer are identified in Figure 2.10 through the variations of heat transfer coefficient (HTC) and wall temperature (T_w) with bulk fluid enthalpy for upward flow of SCW in a straight smooth and vertical tube [13].

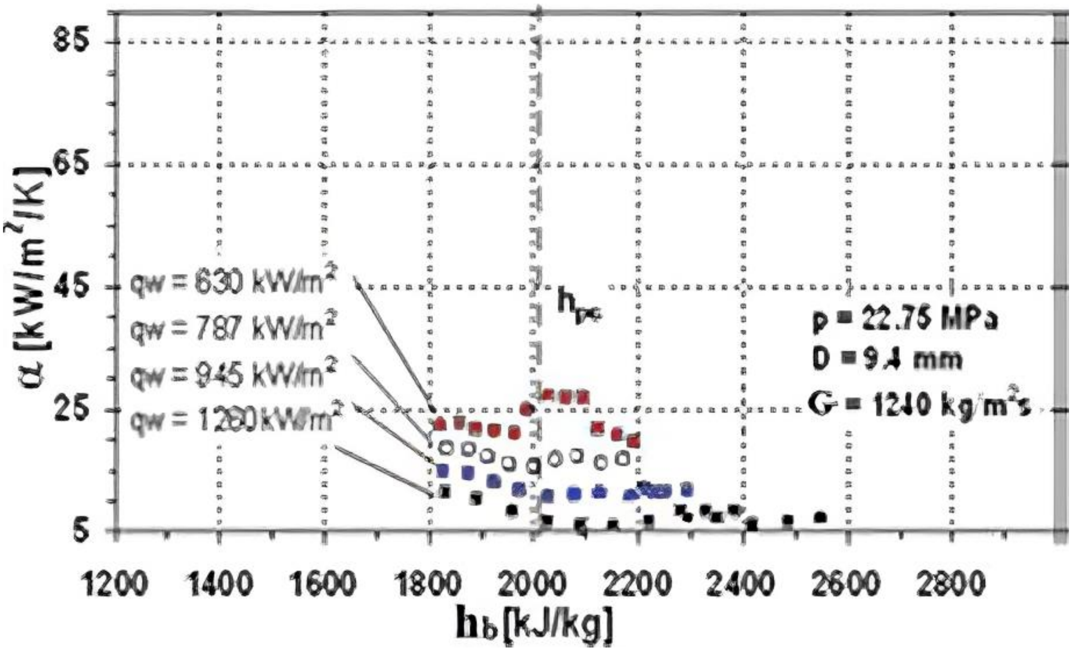

(a) HTC (α) versus h_b

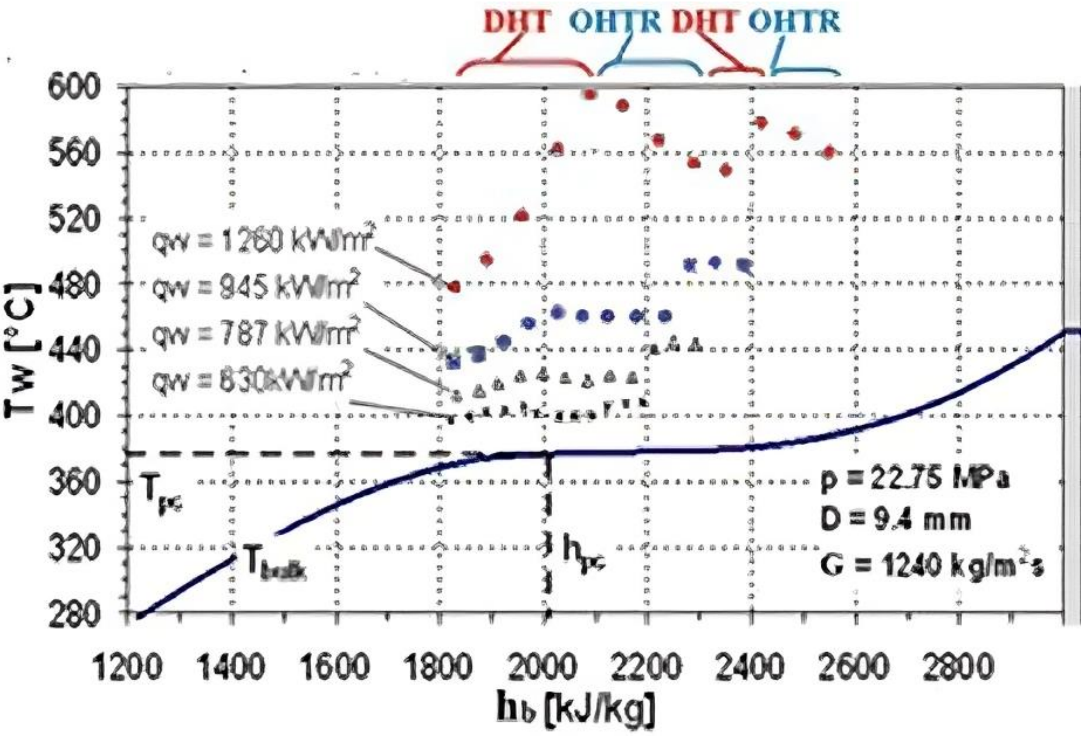

(b) T_w versus h_b

Fig. 2.10 - Experimental results for different heat transfer regimes: EHT (630 kW/m^2), NHT (787 and 945 kW/m^2) and DHT & OHTR (1260 kW/m^2).

2.2.4. Deteriorated heat transfer

DHT is a phenomenon resulting in an increase in the wall temperature resulting from a reduction in the HTC at a heated wall [14][15]. The most contributing factors to DHT occurrence are the heat flux, mass flux, and the geometry, many authors attribute the ratio of heat to mass fluxes (q/G) to be a major factor for the onset of DHT [15] [16] [17]. It is known that DHT is caused by local changes in thermophysical properties of water near the heated wall. [18] argues two means of DHT occurrence, one is when the mass flux is higher than a certain value, while keeping the heat flux constant, the HTC decreases consistently.

The second occurrence is when the mass flux is kept constant at lower than this certain value while increasing the heat flux, the HTC decreases suddenly at certain heat flux values and gradually increases thereafter. [18] claims this is due to the effects of buoyancy forces; when the heat flux increases the buoyancy force becomes stronger near the heated wall leading to a flattening of the velocity profile radially, turbulence is then suppressed and this results in the reduction of the HTC. Once the heat transfer is increased, the buoyancy force undergoes further enhancement, causing a velocity peak near the heated wall, leading to an higher turbulence, because of the newly generated gradient, and the heat transfer is improved again. This means the HTC will be enhanced with mixing; that is when the fluid near the wall mixes with the bulk fluid.

There are some empirical correlations for heat flux calculations at which the deteriorated heat transfer regime appears. One correlation used to highlight the onset of DHT heat flux for a specific mass flux value is suggested by Gabaraev et al. [16], formula (2.3):

$$q_{dht} = 7.9 * 10^{-4} G \left(\frac{P}{P_{rc}}\right)^{1.5} \left[{}^{MW}/_{m^2}\right] \qquad (2.3)$$

2.2.5. Pressure parametric trend

Pressure change in the supercritical region has an effect on the thermophysical properties profiles. The temperature distributions along the wall as well as the centerline temperature were plotted for each case. Figure 2.11 shows the reduction in wall temperatures as the pressure is increased well beyond the critical point. This is due to the fact that the 22 and 23 MPa cases involved water which has already developed past the pseudocritical point and into the dense gas-like region, so the water in these regions has low thermal conductivity insulating the inner surface of the tube, raising the temperature.

An interesting effect observed is that once the pressure reaches 24 MPa, changes in the wall

temperature distribution for subsequent pressures becomes minimal. Because the changes in the properties of the water in the region past the critical point but before the pseudocritical point are much less pronounced. This effect can be seen in specific heat trends as shown in Figure 2.12.

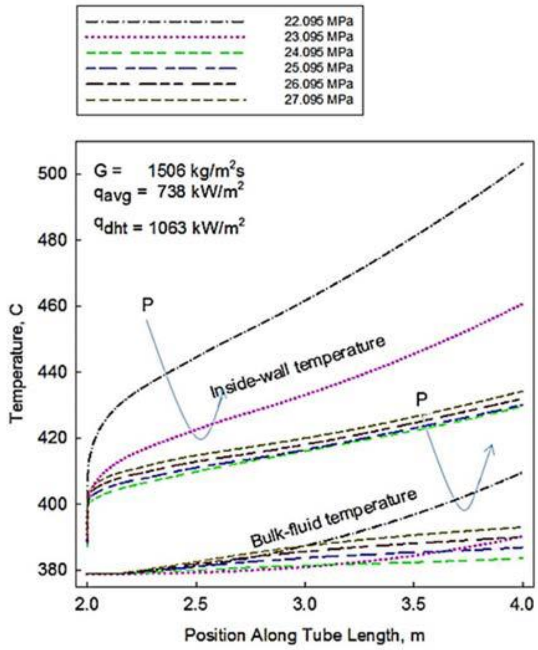

Fig. 2.11 - Pressure variation effect on bulk fluid and wall temperature distributions.

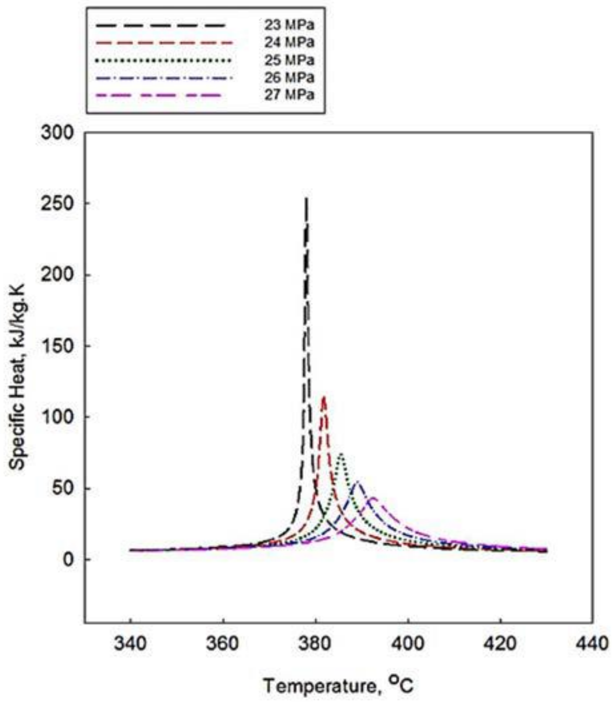

Fig. 2.12 - Specific heat trends with pressure variation.

2.2.6 Development of new correlations for heat transfer to supercritical pressure fluids

For heat transfer in forced convection and fully developed, with fluid at a specified pressure above the critical value, the correct dimensionless parameters for correlating experimental data are Reynolds number, Prandtl number and thermal loading parameter. So a functional relationship of the form as in formula (2.4) is applicable:

$$\left(\frac{q_w D}{k_b (T_w - T_0)}\right) = \Psi \left[\left(\frac{u_b D}{v_b}\right), \left(\frac{\mu_b c_p}{k_b}\right), \left(\frac{q_w D}{k_b T_b}\right)\right] \tag{2.4}$$

where Ψ represents that is function of the argument following.

The thermal loading parameter affects the magnitude of the temperature variation within the fluid and, therefore, the extent of the non-uniformity of fluid properties.

In 1975 by Jackson and Hall [20] (see also Jackson and Hall [21]) reported an evaluation of equations for forced convection heat transfer to fluids at supercritical pressure. Sixteen equations were used to calculate heat transfer coefficients for approximately 2000 different experimental conditions. The differences between calculated and experimental values were evaluated and tabulated [21]. The approach of Krasnoschekov and Protopopov [22] proved to be the most effective. A modified form of it, where the constant properties forced convection equation of Petukhov and Kirillov [23] was replaced by a simpler Dittus-Boelter type expression (formula (2.5)):

$$Nu_b = 0.023\, Re_b^{0.8}\, Pr_b^{0.4} \left(\frac{\rho_w}{\rho_b}\right)^{0.3} \left(\frac{c_p}{c_{p_b}}\right)^{n_2} \tag{2.5}$$

The value of the index n_2 in the specific heat ratio term depends on the values of T_w and T_b in relation to the pseudo-critical value T_{pc} and is determined using the equations specified by Krasnoschekov and Protopopov in Table 2.1.

Table 2.1 - equations by Krasnoschekov and Protopopov

$n_2 = 0.4$	for $T_b < T_w < T_{pc}$ and for $1.2\, T_{pc} < T_b < T_w$
$n_2 = 0.4 + 0.2\, ((T_w/T_{pc}) - 1)$	for $T_b < T_{pc} < T_w$
$n_2 = 0.4 + 0.2\, ((T_w/T_{pc}) - 1)\, (1 - 5\, ((T_b/T_{pc}) - 1))$	for $T_{pc} < T_b < 1.2\, T_{pc}$ and $T_b < T_w$

The index n_2 was approximately 0.4 for many of the conditions covered in the evaluation exercise. However, a better compromise in terms of all round performance was obtained using the following simplified version of formula (2.5), the formula (2.6), where a constant value of 0.4 is used for n_2, and $\overline{Pr}_b = \mu_0 \, \bar{c}_p \, / \, k_b$ (see Jackson and Hall [21]).

$$Nu_b = 0.023 \, Re_b^{0.8} \, \overline{Pr}_b^{0.4} \left(\frac{\rho_w}{\rho_b}\right)^{0.3} \tag{2.6}$$

2.3 Pressure loss characteristics of supercritical water

Pressure losses in the heat-transport system have a direct impact on the pump capacity and the power output, affecting the capital and operating costs. Also, these losses affect the local flow conditions changing the heat-transfer characteristics. The pressure loss components consist of frictional loss, concentrated losses like valves and elbows, head loss for gravity, and loss due to acceleration. The overall pressure loss in the heat-transport system can be expressed as in the formula (2.7)

$$\Delta P = \sum \left(\frac{f}{2}\frac{L}{D}\frac{G^2}{\rho_{avg}}\right)_i + \Delta\left(\frac{G^2}{\rho}\right) \pm \rho_{avg} g L \sin\Theta + \sum \left(K\frac{G^2}{2\rho}\right)_i + \cdots \tag{2.7}$$

where:

f is the friction factor over the pipe section,

L is the length of the pipe section, D is the pipe diameter,

G is the local mass flux in kg/m·s,

g is the gravitational constant (= 9.806 m/s^2),

K is the local form-loss coefficient (for valves, elbow, bend, sudden contraction, sudden expansion, etc.),

θ is the pipe inclination angle to the horizontal plane,

ρ and ρ_{avg} are the local and average densities in kg/m^3.

The sign for the gravitational term changes with '+' referring to the upward flow and '–' to the downward flow.

2.3.1 Frictional pressure drop

There is a lot of experimental work for heat transfer using supercritical fluids and pressure loss data were obtained over the test section as part of the experiments [9]. Pressure loss measurements were reported without key parameters like surface roughness and wall conditions) making it difficult to apply the information. The assumption of a smooth tube is not correct as the corrosive behaviour of supercritical fluids usually leads to a rapid change in surface conditions.

[24] proposed a number of friction factor correlations for tube flows. The most common correlations are the Blasius and the Colebrook and White (C-W) equations [25]. The Blasius friction factor equation, formula (2.8) is based on the assumption of fully developed turbulent flow in a smooth tube:

$$f_{Blasius} = \frac{0.316}{Re_b^{1/4}} \tag{2.8}$$

It is applicable for bulk Reynolds numbers (R_{eb}) up to 105. The C-W friction factor equation, formula (2.9), is applicable for turbulent flow and takes into account the surface roughness [26]:

$$\frac{1}{f_{C-W}^{1/2}} = -2log\left(\frac{\varepsilon/D}{3.7} + \frac{2,51}{Re_b\sqrt{f_{C-W}}}\right) \tag{2.9}$$

2.3.2 Local pressure loss

Local pressure losses due to piping components (such as valves, elbows, bends, etc.) and fuel assembly appendages (such as spacer grids) are calculated with the formula (2.10)

$$\Delta P_{form} = K\frac{G^2}{2\rho} \tag{2.10}$$

The loss coefficient, K, is established by experimental data. Limited information are reported in available literature on loss coefficients for various piping components in supercritical flow.

2.4 Instability and natural circulation in supercritical pressure systems

2.4.1 Introduction

Stability and natural circulation phenomena observed in single-phase conditions at subcritical pressures become more complex at supercritical pressures because of the strong variability of thermodynamic and thermophysical properties. In single-phase flow, instabilities mostly happen in natural circulation systems, being driven by a mechanism explained by Welander [27]. In that study, it was suggested that pockets of fluid with perturbed temperature may come out from the heat source and/or the sink, affecting the fluid residence time along the loop and being damped or amplified for passing through the heater and the cooler. A feature of the observed behaviour is its chaotic character, mainly caused by the fact that the growth of flow perturbations frequently leads to flow reversal. Two-phase flow instabilities are mainly connected with the behaviour of boiling channels that are recognized to be susceptible to different instability mechanisms, having a 'static' or a 'dynamic' nature. The discernment among the two categories of instabilities is introduced considering if their occurrence can be explained on the basis of the static internal pressure drop vs. flow characteristic of the system. The Ledinegg instability mechanism [28] is representative of the category of static instabilities, while density-wave, pressure drop oscillations and thermal oscillations are mechanisms which belong to the second category. Of these instabilities, density waves represent the most relevant instability mechanism for nuclear reactor applications since, in combination with neutronic feedback, it is responsible for observed space and time oscillations of Boiling Water Reactor (BWR) core power.

2.4.2 Natural circulation and flow stability

As the supercritical fluids experience a steep change in their thermodynamic and transport properties (as density, viscosity, specific heat) in the pseudocritical region, the SCW circuit could undergo density wave instability. The drastic change in the density in the pseudocritical region has strong effects in the buoyancy and acceleration, causing changing in the flow and heat transfer behavior. In view of the above, design of SCW circuits poses many challenges with respect to certain thermal hydraulic characteristics for which a confidence level has been developed for the presently operating fleet of reactors which make use of fluids at subcritical pressures either in single phase.

2.4.3 Lesson learned

It has been noted that increasing the power-to-flow ratio leads to instability, with a threshold value that depends on the pseudo subcooling. For example, at a dimensionless subcooling with respect to the pseudocritical temperature ratio of 1, power-to-flow after 1,5 begin to be unstable. While the effect of distributed friction was found minor in the range for the considered loop, it must be remembered that friction actually determines the flow rate as a function of power, thus directly affecting the power-to-flow ratio. The stability boundary obtained by the simplified theory is strongly affected by the presence of the pipe wall structures, having the effect to damp perturbations, favouring stability. The latest observation justifies the difficulties met in predicting stability in actual natural circulation loops, when adopting heat transfer correlations not suitable for deteriorated heat transfer prediction. In fact, on one hand the presence of heating structures tends certainly to stabilize the dynamics, though on the other hand this effect is quantitatively uncertain owing to the present uncertainties in evaluating heat transfer coefficients.

2.5. Materials and chemistry

All the components for a general SCWRs are required to have sufficient strength and to avoid degradation or deformation at high temperatures. The greater degradation mechanisms of SCWR materials are general corrosion, environmental assisted cracking, like stress corrosion cracking (SCC), corrosion fatigue, and radiation embrittlement. Deformation can be induced primarily by void swelling and/or creep. From this point of view, zirconium alloys cannot be used because these alloys do not have enough strength at high temperatures (its yield strength rapidly decreases at temperatures above 500 °C) and also because it has very low resistance to general corrosion (it corrodes easily at temperatures above 400 °C). In order to select materials feasible with both supercritical water and lead, the effects of environment, stress and manufacturing processes need to be evaluated. A certain experience has been obtained from R&D on material development and operation of supercritical fossil fuel power plants and nuclear reheated steam cycle systems [29][30][31]. The first reference has identified, evaluated and qualified the materials needed for the construction of the critical components of coal-fired boilers, operating at 760 °C and 35 MPa steam. These candidate materials were Haynes 230, Inco 740, CCA617, HR 6W, Super 304 H. The study explores the economic viability, candidate alloys applicable to various ranges of temperature and stress rupture tests. Steam-side oxidation tests in an autoclave at 650 and 800 °C have been completed. The second reference identify a short-list of candidate materials for longer-term testing, making available a large amount of data on materials properties (such as corrosion and creep) under SCWR conditions (for temperature between 374 and 732 °C, P = 35 MPa). The paper describes the development of the database made to facilitate the collection and assessment of these data.

2.5.1. General corrosion and stress corrosion cracking (SCC)

When the facility is operating, oxides will buildup on the cladding surface for the corrosion and deposition of corrosion products originating in the feed-train. Small amounts of oxide formation on the cladding surface will increase the roughness and may enhance convective heat transfer from the surface to the coolant. However, significant oxide buildup reduces heat transfer efficiency by conduction through the cladding leading to increases in cladding and fuel temperatures. In general, the main application for ferritic/martensitic (F/M) steels are the RPV and ex-core components, like piping where temperature is low enough (≤ 400 °C). The modification of existing materials to improve their oxidation resistance can be done via coating of the surfaces or shot peening in order to enhance oxidation resistance through cold working of the surfaces.

2.5.2. Water chemistry

In a supercritical water circuit, water chemistry control is essential for several reasons: the presence of salts and oxides may be aggressive for metal alloys, and the chemistry of water, such as the dissolved oxygen and pH, may induce stress corrosion and accelerated oxidation. If small quantities of impurities deposit on heat transfer surfaces, the heat transfer is reduced, leading to local overheating and thermal cracking issues. For these reasons, demineralization unit and oxygen treatment system are required.

Oxygen Treatment (OT) was initially generated as a feedwater treatment for once-through conventional units with the main purpose to reduce the single-phase flux accelerated corrosion (FAC) and the iron transport from the feedwater. OT adds oxygen and ammonia (since amines are forbidden) to the feedwater. The level of oxygen in water should range in 30 - 200 ppb, proportional with the pH.

Control of pH is needed for several reasons: corrosion of metals and alloys is a function of pH at operating temperature and alkaline pH values increase the stability of iron oxide films, reducing their solubility in water. Control of pH is obtained with an ion specific electrode (ISE). This measurement in high purity water can be difficult with pH measurement technology available [32]. For this reason, it is suggested the continuous verification of pH measurements using relationships between pH and conductivity. The target pH control range for AVT(O) is 9.2-9.8 at 25°C with oxygen control between 5-10 ppb to minimize flow-accelerated corrosion.

Specific conductivity is an online method for monitoring the level of contamination in unconditioned makeup and treatment chemicals water cycle. Due the fact the ammonia injection is higher to contaminant levels usually present, specific conductivity values suggest ammonia concentration and reflect the pH values, and are relatively less sensitive to the level of impurities present. In water where high purity conditions exist and ammonia is used for pH control, the specific conductivity can be used as a direct validation of pH measurements.

Ammonia (NH_3), applied as ammonium hydroxide (NH_4OH) or aqueous ammonia, is the favorite alkalizing agent, being completely volatile and not subject to thermal decomposition at the superheated steam temperatures of 538 °C at subcritical and supercritical pressures.

An alternative approach for measuring pH, dissolved oxygen and conductivity is to employ a single multi-input analyzer that can handle several probes, whether they are pH, DO or conductivity sensor. These analyzers are capable of receiving signals from two or more probes simultaneously and are readily available from most manufacturers. This configuration allows each sample point to have its own dedicated measuring sensor.

Several conventional supercritical units tend to develop high-temperature duplex oxides on the low-alloy tubing of Oxygen Treatment unit waterwalls. This oxide formation naturally occurs under high-temperatures conditions (greater than approximately 400 °C). In some cases, chemical cleaning may be necessary to eliminate these oxide layers [33].

To resume, the main goal is to passivate metal surface in order to prevent corrosion. The main chemical product used are: deoxygenating agent, to remove dissolved oxygen, volatile alkalizing agents, to maintain the optimal pH and stabilizer of encrusting salts, used to keep salts in suspension and prevent scale formation. During start-up phase, a manual or automatic dosing system is recommended, with the possibility of regulation due to the high variability of operating conditions. Once steady-state operation is reached, a continuous dosing system can be evaluated.

3. Versatile Loop Facility

The Versatile Loop Facility (VLF) is an experimental installation developed by Ansaldo Nucleare as part of the Westinghouse Electric Company Lead Fast Reactor (WEC-LFR) program. Its primary objective is to investigate the thermo-hydraulics behavior of liquid lead under operational conditions, particularly coupled with supercritical water cooling in the secondary loop [35]. Within the framework of the VLF, emphasis is placed on the testing and assessment of the Primary Heat Exchanger (PHE) and the Fuel Pin Bundle Simulator (FPBS).
The WEC-LFR is a 465 MW_e, pool type, passively safe, fast neutron reactor cooled by liquid lead [36]. The Reactor Vessel (RV) adopts integral configuration, in which all primary system components are housed internally [37]. The primary pool is equipped with compact hybrid microchannel heat exchangers designed to transfer heat from the lead coolant to the supercritical water of the secondary system. Owing to their high heat transfer area to volume ratio, these microchannel exchangers provide significant compactness, reducing the RV size while enhancing system robustness. Moreover, their structural characteristics nearly eliminate the risk of pressurization accidents within the nuclear system.

3.1 Primary system description

Figure 3.1 illustrates the primary loop of the VLF. The system consists of a liquid-lead circuit that function as the facility's primary coolant loop. Heat is supplied to the lead within the FPBS, which emulates the behavior of a conventional nuclear fuel assembly through the use of electrical heating rods. The primary coolant enters the component at 390 °C, while the outlet temperature in the hot leg varies as a function of both the applied power and the mass flow rate. Under nominal conditions, the outlet temperature is maintained at approximately 530 °C, with the possibility of extending up to 650 °C. Subsequently, the heated lead is cooled within the Primary Heat Exchanger by means of supercritical water on the secondary side. The fluid then returns to the main tank, from which it is recirculated into the cold leg by a centrifugal pump, thus completing the loop [37]. To ensure operation reliability, the entire primary circuit, including its major components, is equipped with trace heating and thermal insulation. These measures are designed to regulate temperature during start-up operations and to prevent the solidification of lead. The overall installed capacity of the system is approximately 500 kW.

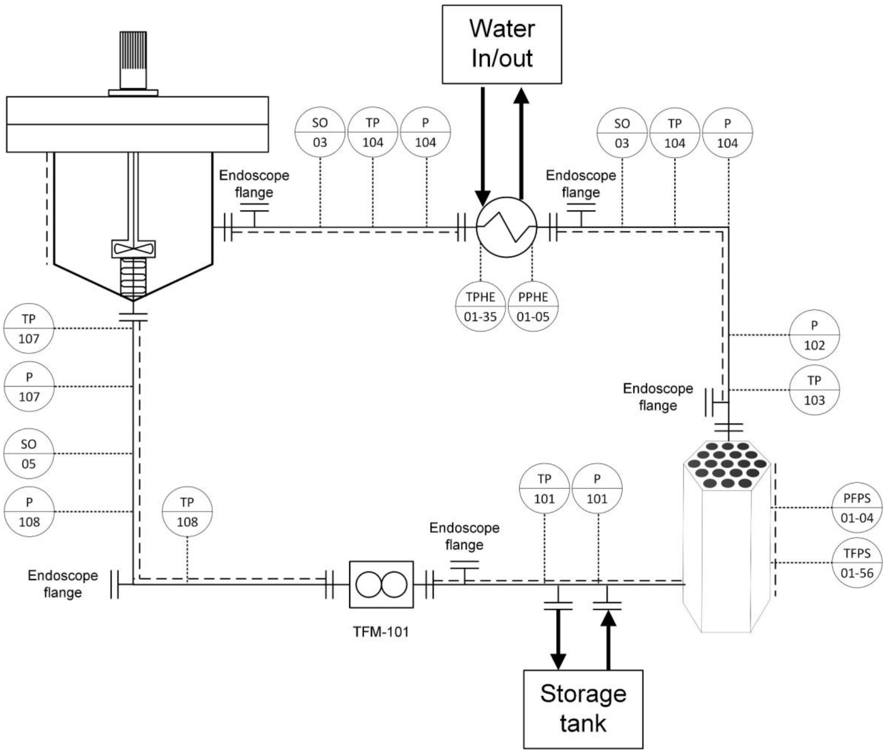

Fig. 3.1 – Primary system

3.2 Secondary system description

The original VLF layout is an open circuit: the reasons behind the choice of a closure are several. First of all, less water losses can be achieved, having the same water recirculating, leading to a less dependence on external availability. In second instance, less air and impurities can enter the system, allowing reaching less corrosion and incrustations. At last, avoiding water-atmosphere contact can prevent bacterial proliferation.
The secondary loop of the VLF is configurated as an open supercritical water circuit. Its function is to extract heat from the lead within the PHE and to transfer the removed thermal power to the heat sink. A schematic representation of the system is provided in Figure 3.2.

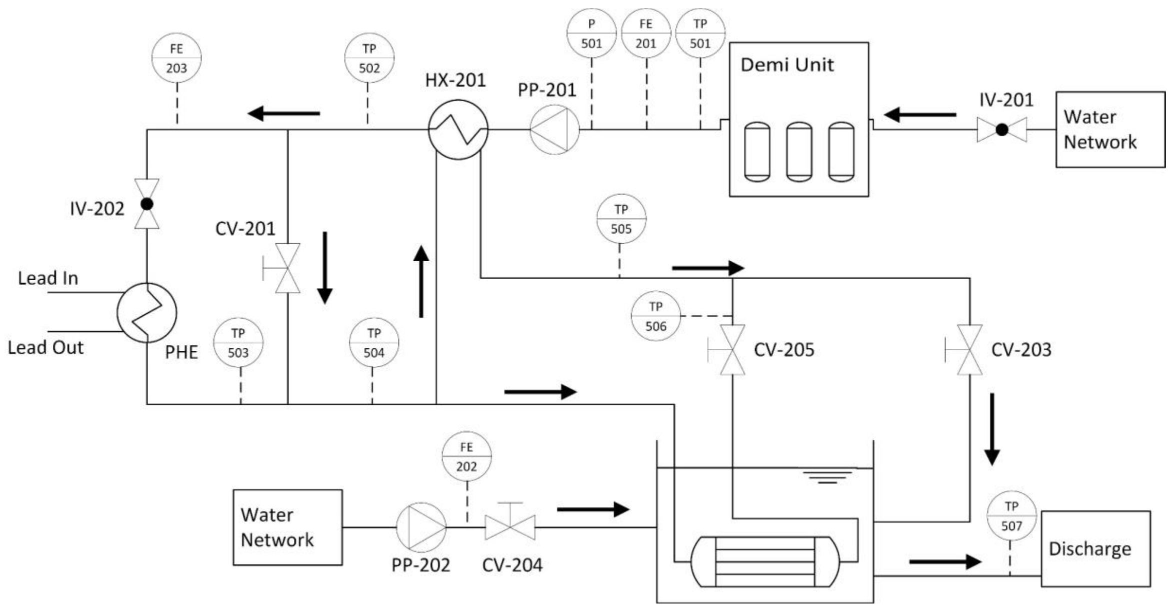

Fig. 3.2 – Secondary system

The secondary coolant is supplied from the water network at 20 °C and, after undergoing demineralization, is pressurized by a volumetric pump (PP-201), which compresses the fluid through pistons up to a pressure of 300 bar. Subsequently, the supercritical water passes through a regenerative microchannel heat exchanger (HX-201), where is heated to approximately 350 °C.

At this stage, the total mass flow divides into two branches: one directed towards the PHE and one bypassing it. The division of the flow is governed by the control valve CV-201, which regulates the distribution so as to maintain a constant outlet temperature of 480 °C (extendible up to 600°C) from the PHE. Downstream of the PHE, the two flows path recombine at 430 °C and are then split again in two separate branches: one directed to the hot side of the HX-201, and the other into a serpentine heat exchanger submerged in a tank (TK-202). Flow rates in these branches are regulated by control valve CV-205, positioned at the serpentine outlet, in order to stabilize the HX-201 cold-side outlet temperature. Once recombined, the coolant at 90 °C is depressurized to near-ambient conditions via CV-203, thereby ensuring constant pressure downstream of PP-201. The fluid is then discharged into TK-202.

To guarantee a stable thermal state within the tank, a continuous refill of mass flow is maintained, controlled by CV-204, which discharges the fluid approximately at 60 °C. The piping system is designed to limit the flow velocity to 4 m/s. All regulating devices are globe-type valves, differentiated by diameter and flow coefficient [38]. Safety relief valves are integrated into the loop to prevent overpressure transient during nominal operation or accidental conditions (such as fire events). The relief system is calibrated to open at 320 bars, discharging excess water safely intro the external environment. During overpressure transient, relief valves operate in coordination with the pump monitoring system and valve CV-203, which is designed to fully open under failure conditions. Furthermore, two isolation valves are installed: IV-202, located upstream of the PHE, and IV-201, positioned downstream of the water network connection.

4. RELAP5

4.1 RELAP5 System Code

RELAP5 is a thermal-hydraulic system code created at INL (Idaho National Laboratory). The source code, written in Fortran 77, is widely used by research institutions. The main purpose of RELAP5 is to solve one-dimensional fluid-dynamic problems, particularly those involving heat transfer.
The code allows users to divide a plant into control volumes that represent the available space for fluid flow. These control volumes are linked by junctions that permit fluid transfer between them. In each system, only one fluid can be chosen, which may be single-phase or two-phase, with the possibility of adding non-condensable gases and boron.
RELAP5 solves the conservation equations of mass, energy and momentum. For each control volume, scalar quantities such as temperature or pression are calculated at its center, while vector quantities like velocity are defined at boundaries. The solution is obtained through time-step integration to capture transient behavior [39].
There are different hydrodynamic components available for system simulation:

• Single Volume (SNGLVOL): represents a single control volume

• Single Junction (SNGLJUN): represents a junction between two control volumes

• Pipe (PIPE): interconnects many volumes with internal junctions

• Time Dependent Volume (TMPDVOL): it's a control volume which imposes fluid thermodynamic conditions (e.g., pressure, temperature) during the simulation evolution

• Time Dependent Junction (TMDPJUN): allows the user to impose the time variation of a physical quantity. In a TMDPJUN velocity and mass flow rate are established

• Valve (VALVE): it's a junction that variates its area like a valve. The user can insert the valve flow coefficient as a function of the normalized area to properly simulate the valve

Every plant's solid structure, such as fuel rods, heat exchanger, pipes, are modeled in RELAP5 as heat structure. These components are able to simulate heat transfer processes, including conduction, convection and radiation, between the fluid and the walls of the system. Several built-in heat transfer correlations are available, but the user can provide customized data tables. Either predefined correlations can be used, or user-supplied tables can be introduced in the input deck. Mesh spacing within solid domains is defined on the degree of resolution required. The user may also define multiple mesh point to obtain a more accurate temperature distribution along the solid domain.
RELAP5 also provides the capability to carry out mathematical and logical operations through control variables and trips, inserted into the input deck by means of special cards. Control variables allow the user to perform algebraic operations on variables, while trips define logical conditions. This mechanism is essential for simulating automatic safety system responses such as valve actuation. Logical relations between trips can also be defined using Boolean operators like AND, OR and XOR, thus enabling the creation of complex conditions.

4.2 RELAP5 VLF nodalization description

In the VLF facility the different objects have been modelled following the suggested components of RELAP5. While in a CFD analysis a thick mesh in needed to know parameters in every point, RELAP5 presents *nodes*, allowing less calculation power to reach a solution. The number of nodes depends on the need to know the values at that point, so a heat exchanger will be modeled with 85 nodes, while a short pipe with just two.
The section of the system between the triplex pump (PP-201) and the discharge line of tank TK-202 of the secondary loop was copied in the model from the 3D CAD geometry of the facility. The geometric layout was preserved, and pressure drop were calculated using RELAP5 wall friction correlations.
Tank TK-202 was represented as a large vessel simulated with three parallel pipe components, each modeling the buoyancy effect of the tank's internal volume. Heat exchangers and other cross-junction components were also included to match the plant's geometry. Their hydraulic behavior was calibrated according to plant data.
The overall nodalization scheme of the VLF secondary loop is presented in Figure 4.1. The figure provides an overview of the layout, but the actual 3D geometry is not fully represented. In particular, length and volumes appear distorted due to the 2D projection, so the figure should not be interpreted as exact in terms of dimensions.

The first digit of the hydrodynamic components number identifies a specific system as follows:

• "1XX" for the piping of the primary loop and the PHE lead side

• "2XX" for the PHE supercritical water side

• "3XX" for the piping of the secondary loop

• "4XX" for the cold side of the HX-201

• "5XX" for the hot side of the HX-201 and air coolers

• "6XX" for the tube side of the condenser

• "7XX" for the S-101 and the primary pump

• "8XX" for the pool side of the condenser

• "9XX" for the subchannels within the FPBS, for the post depressurization branch and for the pool side cooling branch

In Figure 4.1 the used nodalization for the VLF closed cycle in presented.

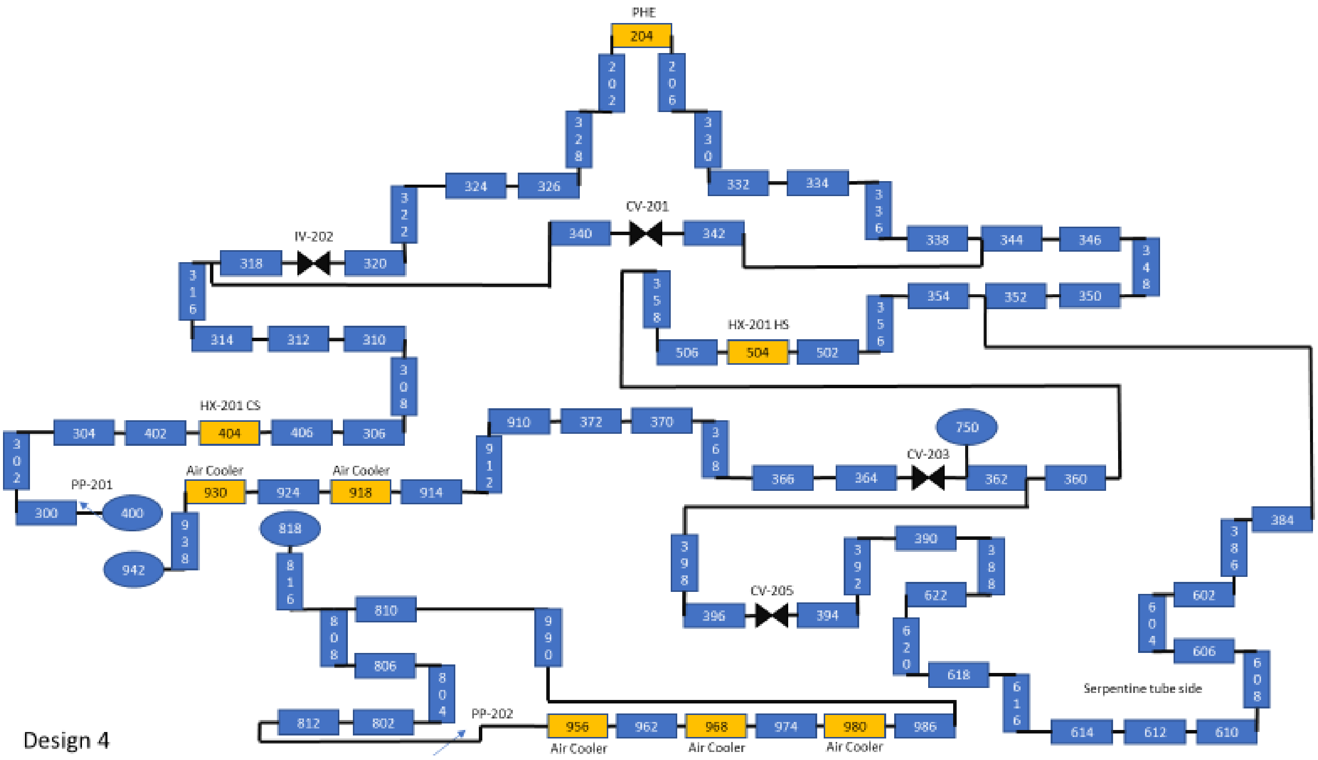

Fig. 4.1 – Nodalization of closed cycle

4.2.1 Pump and Piping

PP-201 secondary pump is modeled by the TMDPVOL 400, raising the pressure of 300 bar in the loop and at temperature of 20 °C, and by the TMDPJUN 401, imposing the mass flow circulating in the loop. PP-202 was modeled in the same way.

Each pipe within the plant sector has been represented by a PIPE component, characterized by its cross-section area and total length. The reference value adopted for the pipe surface roughness is 4×10^{-5} m, while local loss coefficient has been calculated for bends, area variation, inlets and outlets by applying well-established empirical correlation. Pipelines heat losses toward the external environment were simulated by discretizing the pipe wall into 10 radial mesh point for each section. The steel and insulation layers were modeled explicitly, assuming an external boundary condition corresponding to constant ambient temperature of 20 °C and combined heat transfer coefficient of 6 W/m^2K. The adopted HTC value represent the sum of the convective and radiative contribution, determined according to the additivity coefficient method. This reference value was derived from engineering judgment based on similar experimental experiences. All piping sections, expect for the one immersed in low temperature fluid and part of the section connected to the heat sink TK-202, are insulated with 150 mm of rockwood to limit heat losses and maintain thermal efficiency. The piping network connected to the TK-202 heat exchanger, consist of 6 horizontal and 6 vertical segments. Their length and inclination were selected according to the specification of the 3D model.

4.2.2 Valves

The VLF secondary loop has four control valves, two isolation valves and two safety valves. Regarding control valves [9]:

• CV-201: 1'' globe control valve situated at the PHE bypass, controlling the mass flow through the PHE, keeping its outlet temperature constant.

• CV-203: 1'' globe control valve, it depressurizes water to atmospheric pressure. It is located at the merging of the circuit before the tank dump.

• CV-204: 1 ½'' globe control valve. It is situated in the refill line, keeping the tank water outlet temperature constant at 60 °C.

• CV-205: 1'' globe control valve, it is installed downstream the serpentine, regulating the mass flow split between the HX-201 branch and the serpentine.

All the control valves are modelled with "VALVE" components considering the C_v curves specified by the manufacturer.

4.2.3 Heat exchangers

The PHE and the HX-201 are compact, diffusion-bonded heat exchangers. They are constituted by several stacked plates, each one with its own flow area. The heat exchangers were modeled as equivalent PIPE components, each representing the full length of a single channel. However, to ensure proper pressure distribution, a concentrated pressure loss was added to the pipe component corresponding to each heat exchanger [39]. The total number of tubes, channel diameters, and pitch were estimated from available reference data.
Assuming the channels are straight, plate-type geometry was adopted to simplify the calculation of the thermal and hydraulic performance. A preliminary estimate of the overall heat transfer area was then obtained for both the primary and the secondary sides of the heat exchangers. The nominal heat transfer coefficients were calculated using the Dittus-Boelter correlation implemented in RELAP5.
Since the actual thermal-hydraulic structures of the exchangers were not fully characterized, corrective factors, commonly known as fouling factors, were introduced to match the model output with available experimental data. These factors were applied to both primary and secondary side heat transfer coefficient to better reproduce the expected temperatures and flow rates. This calibration method has been successfully used in previous works to improve the consistency between RELAP5 simulations and experimental results. The heat exchange is ensured by coupling the two pipes lines, creating a heat structure and defining material and surface area through the *safac* (surface area factor).

5. Closed loop conceptualization

In this chapter different design concepts are presented for the closure of the secondary cycle, facing the pros and cons of each. Every design requires a chemistry control system and an expansion vase.

5.1 Design 1

In this conceptualization tank-202 and the serpentine are removed, passing all the flow rate through the regenerative heat exchanger. This leads to a higher hot temperature of 275 °C at HX-201 hot side exit, making necessary to cool down before a safe depressurization. For this reason, several air-cooler are needed, as we can see in Figure 5.1. After the depressurization, water is further cooled with air down to 30 °C.
The positive aspect of this concept is removing of the bulky water tank (2,3x1,15x1,77 m), but the negative aspects are the high number of coolers between 40 and 120 kW needed to cool down the supercritical water and the loss of a bypass line for the regenerator, losing a degree of freedom for the circuit control.

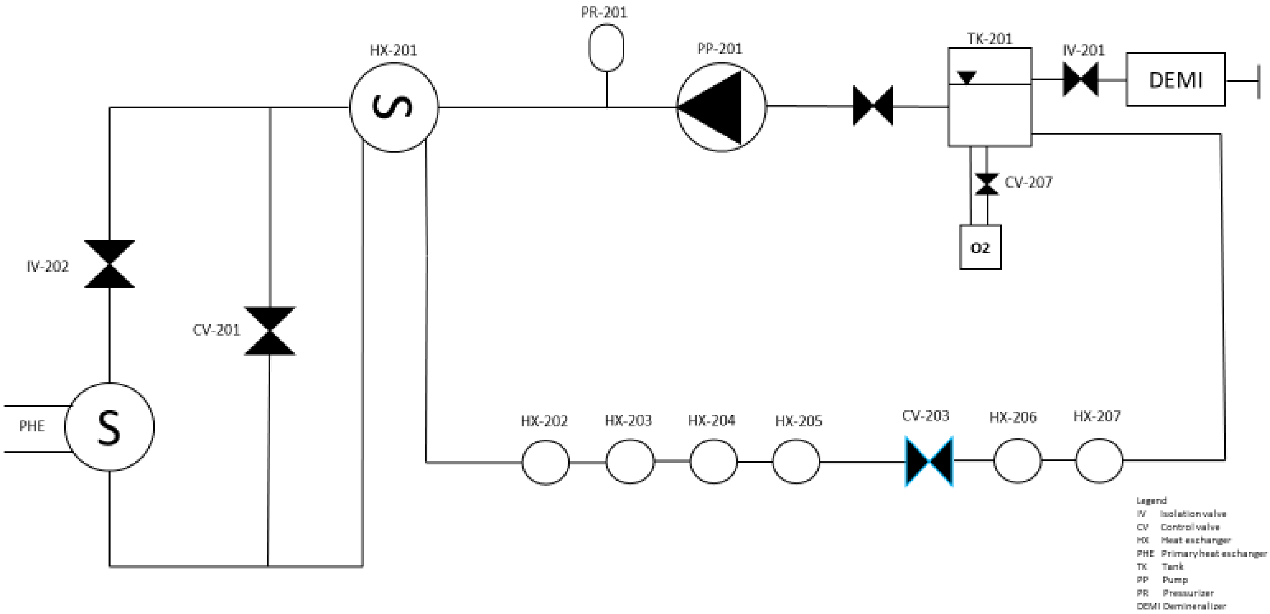

Fig. 5.1 – Design 1

Entering at 30 °C, the following formulas are used to calculate all the cycle points temperatures. Enthalpy in point 2 is calculated with formula (5.1) and the corresponding temperature in formula (5.2).

$$h_2 = h_1(p_1 T_1) + \frac{\dot{q}_{hx201}}{\dot{m}_{hx201}} \tag{5.1}$$

$$T_2 = f(p_2 h_2) = 350\ °C \tag{5.2}$$

Then, enthalpy and the relative temperature of point 3 are calculated with formulas (5.3) and (5.4).

$$h_3 = h_2(p_2 T_2) + \frac{\dot{q}_{phe}}{\dot{m}_{phe}} \tag{5.3}$$

$$T_3 = f(p_3 h_3) = 480\ °C \tag{5.4}$$

Mixed flows enthalpy and its temperature are founded via formulas (5.5) and (5.6).

$$h_4 = \frac{\dot{m}_3 h_3 + \dot{m}_a h_a}{\dot{m}_3 + \dot{m}_a} \tag{5.5}$$

$$T_4 = f(p_4 h_4) = 430\ °C \tag{5.6}$$

Heat flux of HX-201 comes from (5.7).

$$q_{hx201} = \dot{m}_{hx201}(h_2 - h_1) \tag{5.7}$$

Exit temperature at regenerator is found with formulas (5.8) and (5.9).

$$h_6 = h_5(p_5 T_5) - \frac{\dot{q}_{hx201}}{\dot{m}_{hx201}} \tag{5.8}$$

$$T_6 = f(p_6 h_6) = 275\ °C \tag{5.9}$$

Before depressurization, three air heat exchangers of 90 kW each and one of 120 kW are required, with a final temperature as in formula (5.10).

$$T_{10} = f(p_{10} h_{10}) = 96\ °C \tag{5.10}$$

After depressurization, two air coolers of total power of 110 kW are needed to bring water to 30 °C, with a final temperature as in formula (5.11).

$$T_{12} = f(p_{12} h_{12}) = 30\ °C \tag{5.11}$$

In figure 5.2 and table 5.1 are shown point by point the cycle temperatures.

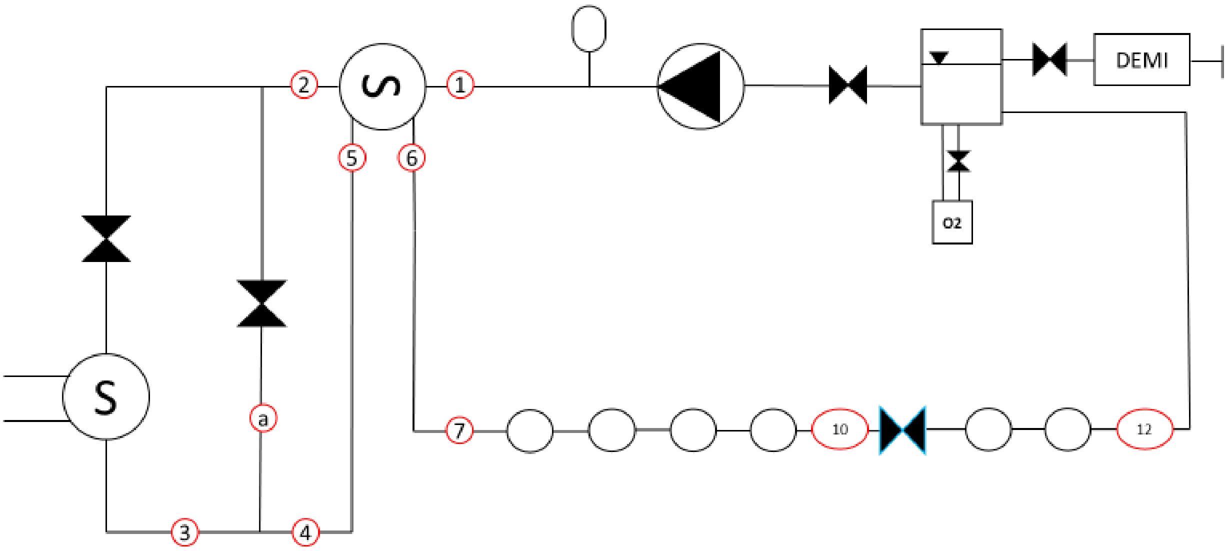

Fig. 5.2 – Design 1

Table 5.1 – Cycle temperatures

Point	Location	p [bar]	T [°C]	m [kg/s]
1	HX-201 cold side ingress	300	30	0,474
2	HX-201 cold side exit	300	350	0,474
3	PHE exit	300	480	0,361
a	Bypass CV-201	300	350	0,113
4	Fluxes from phe and bypass	300	430	0,474
5	HX-201 hot side ingress	300	430	0,474
6	HX-201 hot side exit	300	275	0,474
7	1st air cooler exit	1	235	0,474
8	2nd air cooler exit	1	191	0,474
9	3rd air cooler exit	1	147	0,474
10	4th air cooler exit	1	86	0,474
11	5th air cooler exit	1	51	0,474
12	6th air cooler exit	1	31	0,474

5.2 Design 2

In the second design, as in the first one, the tank and the serpentine are removed, and the supercritical water is cooled down with oil heat exchangers. Oil is then cooled by a tertiary circuit with air cooler, as shown in Figure 5.2. The choice of using oil comes from the capability of this fluid to stay liquid at temperature higher than the vaporization of water (i.e. 100 °C), but the negative side of using an inflammable fluid is the autoignition temperature, leading to security issues. For this reason, a high flash point oil was chosen, the Essotherm 500: this fluid has a maximum operating temperature of 315 °C, a flash point of 200 °C and an autoignition temperature of 380 °C. Four heat exchangers are adopted for a smoother temperature gradient inside each one. Oil is then refrigerated with air coolers. After the depressurization, water is further cooled with air down to 30 °C.
The positive aspect of this design is the HX-201 bypass line maintenance, but introducing a tertiary oil circuit leads to system complication. Water-oil heat exchangers of the required power has indicatively a length of 1000 mm and a diameter of 20 mm. Furthermore, oil tends to deteriorate, so a periodical substitution is suggested.

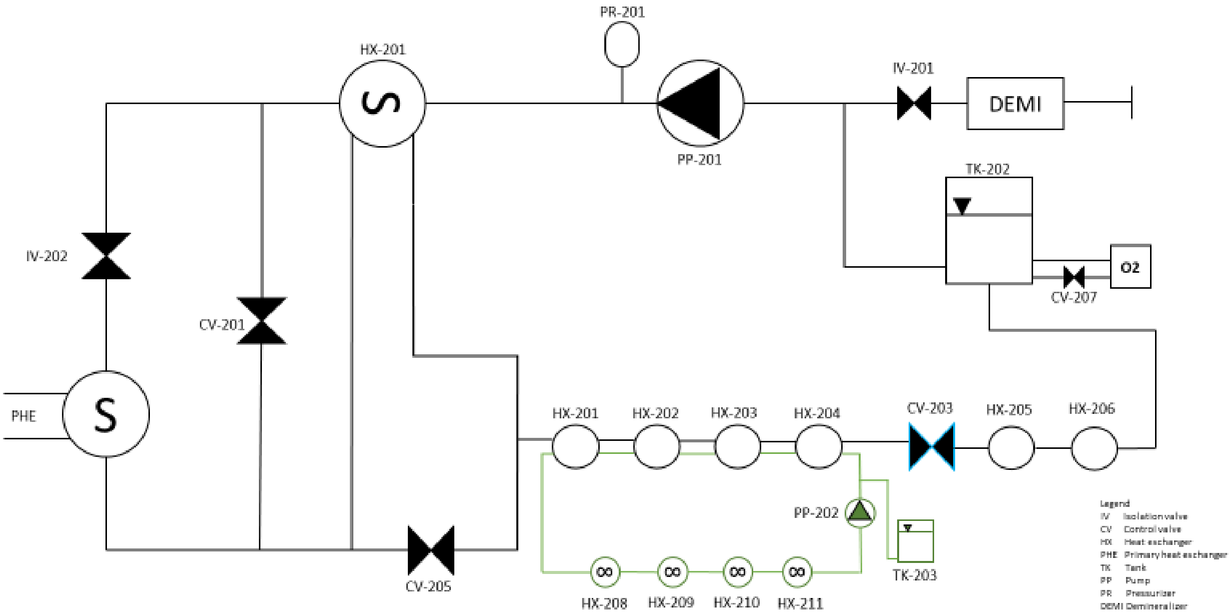

Fig. 5.3 – Design 2

Entering at 30 °C, the following formulas are used to calculate all the cycle points temperatures. Enthalpy in point 2 is calculated with formula (5.12) and the corresponding temperature in formula (5.13).

$$h_2 = h_1(p_1 T_1) + \frac{\dot{q}_{hx201}}{\dot{m}_{hx201}} \tag{5.12}$$

$$T_2 = f(p_2 h_2) = 350\ °C \tag{5.13}$$

Enthalpy and the relative temperature of point 3 are calculated with formulas (5.14) and (5.15).

$$h_3 = h_2(p_2T_2) + \frac{\dot{q}_{phe}}{\dot{m}_{phe}} \tag{5.14}$$

$$T_3 = f(p_3h_3) = 480\ °C \tag{5.15}$$

Mixed flows enthalpy and its temperature are founded via formulas (5.16) and (5.17).

$$h_4 = \frac{\dot{m}_3h_3 + \dot{m}_ah_a}{\dot{m}_3 + \dot{m}_a} \tag{5.16}$$

$$T_4 = f(p_4h_4) = 430\ °C \tag{5.17}$$

Heat flux of HX-201 comes from (5.18)

$$q_{hx201} = \dot{m}_{hx201}(h_2 - h_1) \tag{5.18}$$

Exit temperature at regenerator is found with formulas (5.19) and (5.20)

$$h_6 = h_5(p_5T_5) - \frac{\dot{q}_{hx201}}{\dot{m}_{hx201}} \tag{5.19}$$

$$T_6 = f(p_6h_6) = 267\ °C \tag{5.20}$$

The two branches rejoin at point 8, with a calculated temperature as in formulas (5.21) and (5.22):

$$h_8 = \frac{\dot{m}_6h_6 + \dot{m}_7h_7}{\dot{m}_6 + \dot{m}_7} \tag{5.21}$$

$$T_8 = f(p_8h_8) = 275\ °C \tag{5.22}$$

Each oil heat exchanger cools the supercritical water, removing quite 45 °C every step. The first one is 120 kW of power, while the others are 90 kW. The passages are shown from formula (5.23) to (5.29).

$$q_{hx-oil1} = \dot{m}_{h20}(h_8 - h_A) \tag{5.23}$$

$$T_A = 228\,°C \tag{5.24}$$

$$q_{hx-oil2} = \dot{m}_{h2o}(h_A - h_B) \tag{5.25}$$

$$T_B = 183\,°C \tag{5.26}$$

$$q_{hx-oil3} = \dot{m}_{h2o}(h_B - h_C) \tag{5.27}$$

$$T_C = 138\,°C \tag{5.28}$$

$$q_{hx-oil4} = \dot{m}_{h2o}(h_C - h_D) \tag{5.29}$$

Then, water can be depressurized at temperature T_D, formula (5.30):

$$T_D = 93\,°C \tag{5.30}$$

The diathermal oil heats up with the temperature steps show in formula (5.31) to (5.35):

$$T_F = 30\,°C \tag{5.31}$$

$$T_G = 71\,°C \tag{5.32}$$

$$T_H = 108\,°C \tag{5.33}$$

$$T_I = 147\,°C \tag{5.34}$$

$$T_L = 194\,°C \tag{5.35}$$

After the fourth heat exchanger oil is cooled by other four air coolers.
After a safe depressurization, an addition cooler is required to bring water to 30 °C, calculated by formulas (5.36) and (5.37).

$$q_M = \dot{m}_{h2o}\Delta h_M = 126\ kW \tag{5.36}$$

$$T_M = 30\ °C \tag{5.37}$$

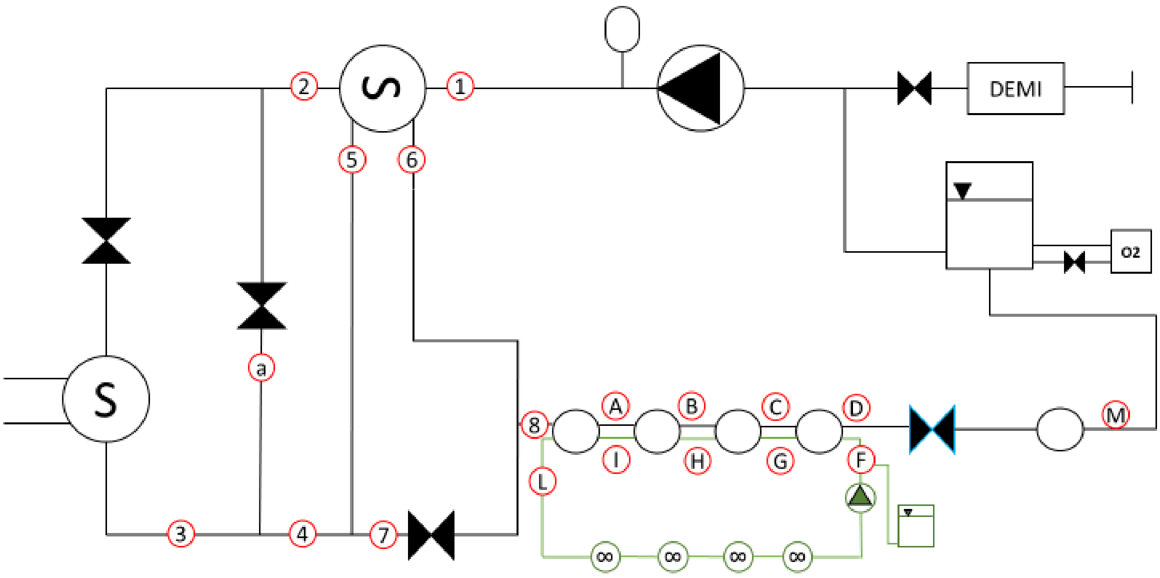

Fig. 5.4 – Design 2

Table 5.2 – Cycle temperatures

Point	Location	p [bar]	T [°C]	m [kg/s]
1	HX-201 cold side ingress	300	30	0,474
2	HX-201 cold side exit	300	350	0,474
3	PHE exit	300	480	0,361
a	Bypass CV-201	300	350	0,113
4	Fluxes from phe and bypass	300	430	0,474
5	HX-201 hot side ingress	300	430	0,314
6	HX-201 hot side exit	300	106	0,314
7	Serpentine ingress	300	430	0,16
8	Fluxes from hx and cv 205	300	275	0,474
A	1st hx exit	300	228	0,474
B	2nd hx exit	300	183	0,474
C	3rd hx exit	300	138	0,474
D	4th hx exit	300	93	0,474
F	4th hx oil side ingress	1	30	1
G	3rd hx oil side ingress	1	71	1
H	2nd hx oil side ingress	1	109	1
I	1st hx oil side ingress	1	147	1
L	1st hx oil side exit	1	194	1
M	hx exit post depr	1	30	0,474

5.3 Design 3

In Figure 5.3 third design is presented. The concept proposed changes the original design the least. Just one more air cooler of 250 kW is needed to cool down water from the tank, the others two are recycled from the open cycle. Then, water at 30 °C is sent to a common tank where the triplex pump and the condenser pump extract their fluid. The TK-202 was open air in the original design, but for a closed cycle external contamination must be prevented, so a closure and a pressurization is needed.
The positive aspects of this concept are several: the basic design is quite the same as the original, the startup procedure remains the same, only a few components have to be purchased.

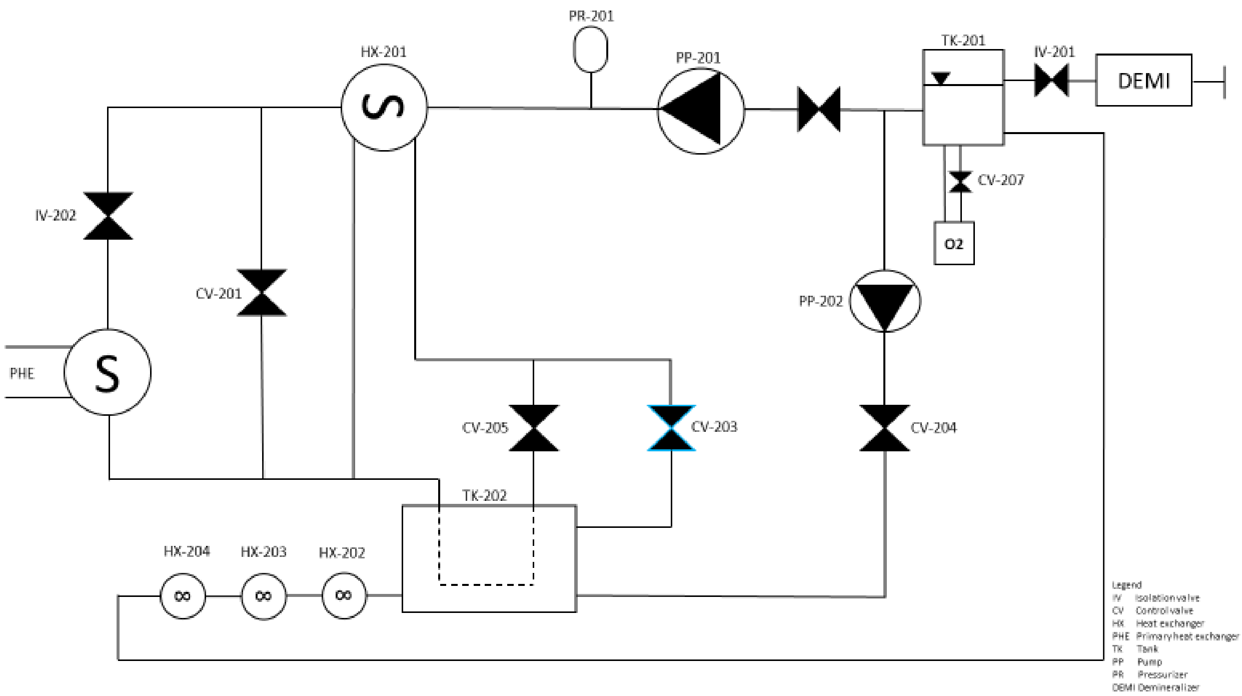

Fig. 5.5 – Design 3

Entering at 40 °C, the following formulas are used to calculate all the cycle points temperatures. Enthalpy in point 2 is calculated with formula (5.37) and the corresponding temperature in formula (5.38).

$$h_2 = h_1(p_1T_1) + \frac{\dot{q}_{hx201}}{\dot{m}_{hx201}} \tag{5.37}$$

$$T_2 = f(p_2h_2) = 350\ °C \tag{5.38}$$

Then, enthalpy and the relative temperature of point 3 are calculated with formulas (5.39) and (5.40).

$$h_3 = h_2(p_2 T_2) + \frac{\dot{q}_{phe}}{\dot{m}_{phe}} \tag{5.39}$$

$$T_3 = f(p_3 h_3) = 480\ °C \tag{5.40}$$

Mixed flows enthalpy and its temperature are founded via formulas (5.41) and (5.42).

$$h_4 = \frac{\dot{m}_3 h_3 + \dot{m}_a h_a}{\dot{m}_3 + \dot{m}_a} \tag{5.41}$$

$$T_4 = f(p_4 h_4) = 430\ °C \tag{5.42}$$

Heat flux of HX-201 comes from (5.43)

$$q_{hx201} = \dot{m}_{hx201}(h_2 - h_1) \tag{5.43}$$

One branch cools down in the regenerative heat exchanger, reaching a temperature as in formula (5.44) and (5.45).

$$h_6 = h_5(p_5 T_5) - \frac{\dot{q}_{hx201}}{\dot{m}_{hx201}} \tag{5.44}$$

$$T_6 = f(p_6 h_6) = 97\ °C \tag{5.45}$$

The second branch cools in the serpentine to temperature obtained with (5.46) and (5.47).

$$h_b = h_7(p_7 T_7) - \frac{\dot{q}_{serp}}{\dot{m}_{serp}} \tag{5.46}$$

$$T_b = f(p_b h_b) = 90\ °C \tag{5.47}$$

The two branches rejoin at point 8 with temperature find by formulas (5.48) and (5.49):

$$h_8 = \frac{\dot{m}_6 h_6 + \dot{m}_b h_b}{\dot{m}_6 + \dot{m}_b} \tag{5.48}$$

$$T_8 = f(p_8 h_8) = 94\ °C \tag{5.49}$$

Mixed flows enthalpy and its temperature are founded via formulas (5.50) and (5.51).

$$h_{tank} = \frac{\dot{m}_9 h_9 + \dot{m}_{10} h_{10}}{\dot{m}_9 + \dot{m}_{10}} \tag{5.50}$$

$$T_{tank} = f(p_{tank} h_{tank}) = 49\ °C \tag{5.51}$$

Water exit the tank at temperature T_A and is cooled by three air coolers, each one with value from formulas from (5.52) to (5.56).

$$h_A = h_{tank}(p_{tank} T_{tank}) - \frac{\dot{q}_{tank}}{\dot{m}_{h2o}} \tag{5.52}$$

$$T_A = 80\ °C \tag{5.53}$$

$$T_B = 60\ °C \tag{5.54}$$

$$T_C = 47\ °C \tag{5.55}$$

$$T_D = 39\ °C \tag{5.56}$$

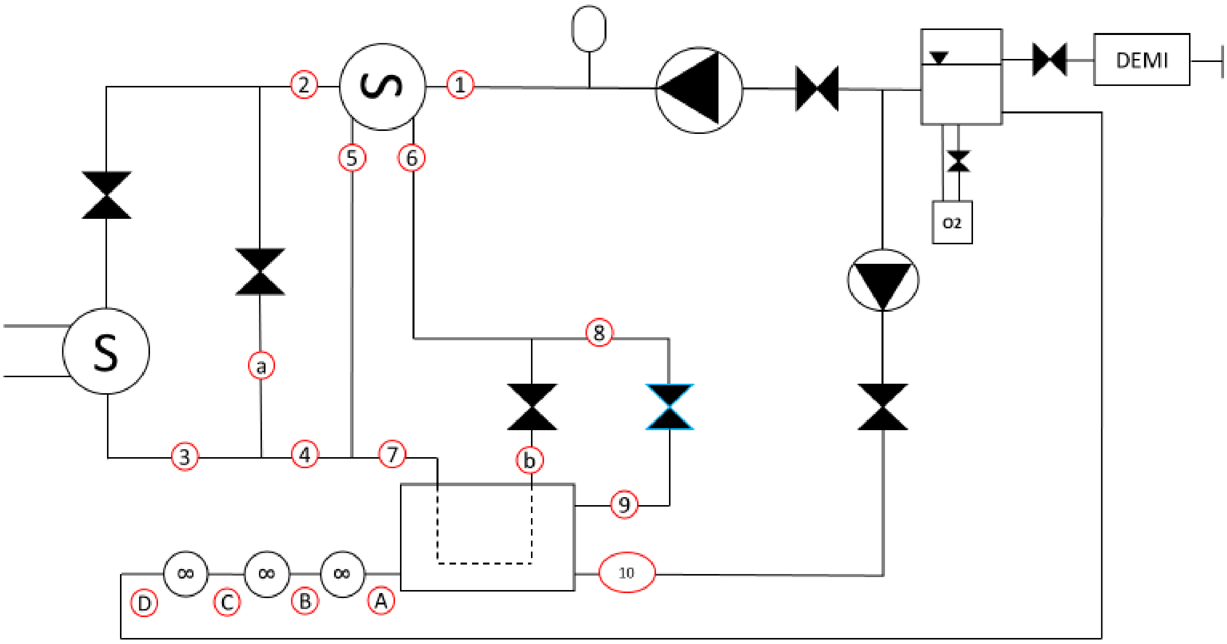

Fig. 5.6 – Design 3

Table 5.3 – Cycle temperatures

Point	Location	p [bar]	T [°C]	m [kg/s]
1	HX-201 cold side ingress	300	40	0,474
2	HX-201 cold side exit	300	350	0,474
3	PHE exit	300	480	0,361
a	Bypass CV-201	300	350	0,113
4	Fluxes from phe and bypass	300	430	0,474
5	HX-201 hot side ingress	300	430	0,3
6	HX-201 hot side exit	300	97	0,3
7	Serpentine ingress	300	430	0,174
b	Serpentine exit	300	90	0,174
8	Fluxes from hx and serpentine	300	94	0,474
9	Tank ingress, depressurized	1	94	0,474
10	Tank ingress, external	5	40	2,5
A	Tank exit	5	80	3
B	1st air cooler exit	5	60	3
C	2nd air cooler exit	5	47	3
D	3rd air cooler exit	5	39	3

5.4 Design 4

The last design proposed in Figure 5.4 is similar to Design 3. After depressurization, water is not sent to the condenser tank, but is cooled down with an air cooler and sent back to the TK-201. The water used for cooling the serpentine is in a third separated loop, chilled by three air coolers, the same type as the open cycle. Having a separate branch allows having more operational flexibility, and demineralized and deoxidized water hasn't to be all the fluid cycle but just the one in the supercritical side. Furthermore, avoiding hotter water entering the tank makes easier to cool it down, so now the higher flow has to be cooled of a minor temperature difference, and the smaller flow rate of an higher temperature difference.

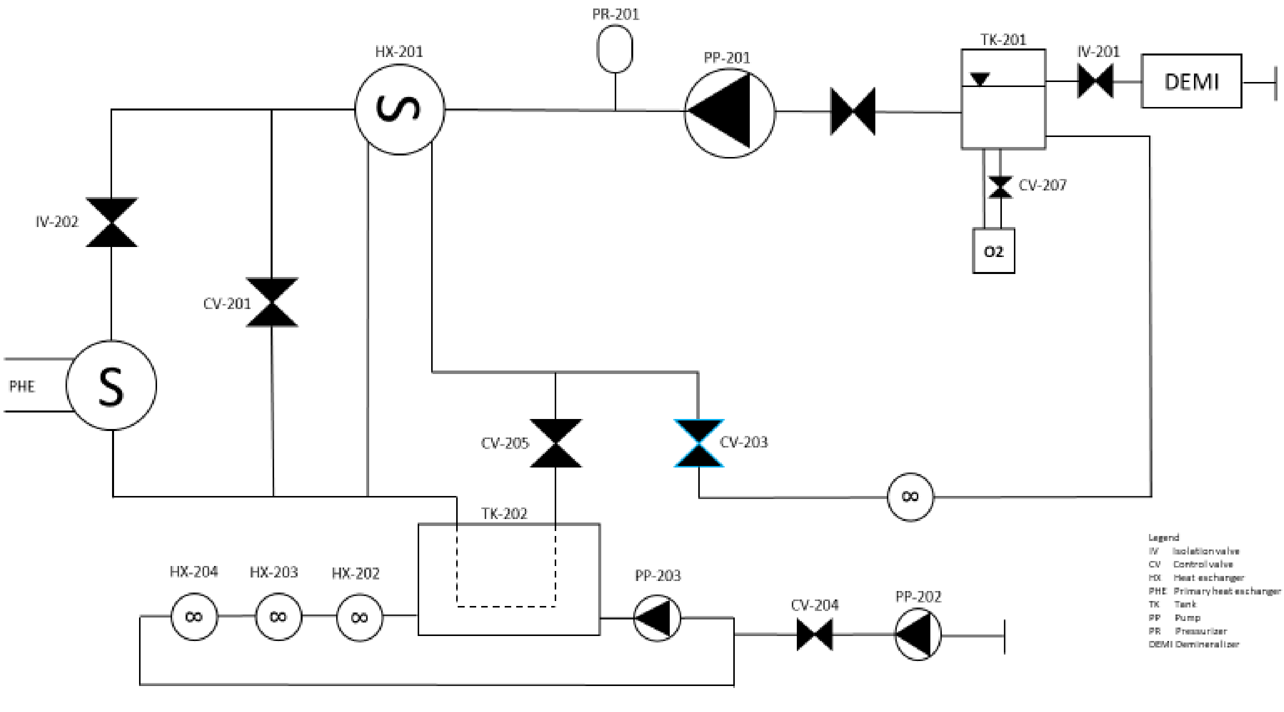

Fig. 5.7 – Design 4

Entering at 30 °C, the following formulas are used to calculate all the cycle points temperatures. Enthalpy in point 2 is calculated with formula (5.1) and the corresponding temperature in formula (5.2).

$$h_2 = h_1(p_1T_1) + \frac{\dot{q}_{hx201}}{\dot{m}_{hx201}} \tag{5.57}$$

$$T_2 = f(p_2h_2) = 350\ °C \tag{5.58}$$

Then, enthalpy and the relative temperature of point 3 are calculated with formulas (5.59) and (5.60).

$$h_3 = h_2(p_2 T_2) + \frac{\dot{q}_{phe}}{\dot{m}_{phe}} \tag{5.59}$$

$$T_3 = f(p_3 h_3) = 480\ °C \tag{5.60}$$

Mixed flows enthalpy and its temperature are founded via formulas (5.61) and (5.62).

$$h_4 = \frac{\dot{m}_3 h_3 + \dot{m}_a h_a}{\dot{m}_3 + \dot{m}_a} \tag{5.61}$$

$$T_4 = f(p_4 h_4) = 430\ °C \tag{5.62}$$

One branch cools down in the regenerative heat exchanger, as in formula (5.63)

$$q_{hx201} = \dot{m}_{hx201}(h_2 - h_1) \tag{5.63}$$

Exit temperature at regenerator is found with formulas (5.64) and (5.65)

$$h_6 = h_5(p_5 T_5) + \frac{\dot{q}_{hx201}}{\dot{m}_{hx201}} \tag{5.64}$$

$$T_6 = f(p_6 h_6) = 97\ °C \tag{5.65}$$

The second branch cools in the serpentine, reaching a temperature obtained with formulas (5.66) and (5.67).

$$h_b = h_7(p_7 T_7) - \frac{\dot{q}_{serp}}{\dot{m}_{serp}} \tag{5.66}$$

$$T_b = f(p_b h_b) = 90\ °C \tag{5.67}$$

The two branches rejoin at point 8, with a temperature by formulas (5.68) and (5.69).

$$h_8 = \frac{\dot{m}_6 h_6 + \dot{m}_b h_b}{\dot{m}_6 + \dot{m}_b} \tag{5.68}$$

$$T_8 = f(p_8 h_8) = 94\,°C \tag{5.68}$$

After depressurization, water is cooled by a 108 kW heat exchanger down to T_9 as in formulas (5.70) and (5.71).

$$h_9 = h_8(p_8 T_8) - \frac{\dot{q}_{vent}}{\dot{m}_{h2o}} \tag{5.70}$$

$$T_9 = f(p_9 h_9) = 30\,°C \tag{5.71}$$

Water exit the tank at temperature T_A and is cooled by three air coolers, each one with value from formulas from (5.72) to (5.76).

$$h_A = h_{10}(p_{10} T_{10}) + \frac{\dot{q}_{serp}}{\dot{m}_{h2o}} \tag{5.72}$$

$$T_A = 68\,°C \tag{5.73}$$

$$T_B = 52\,°C \tag{5.74}$$

$$T_C = 42\,°C \tag{5.75}$$

$$T_D = 31\,°C \tag{5.76}$$

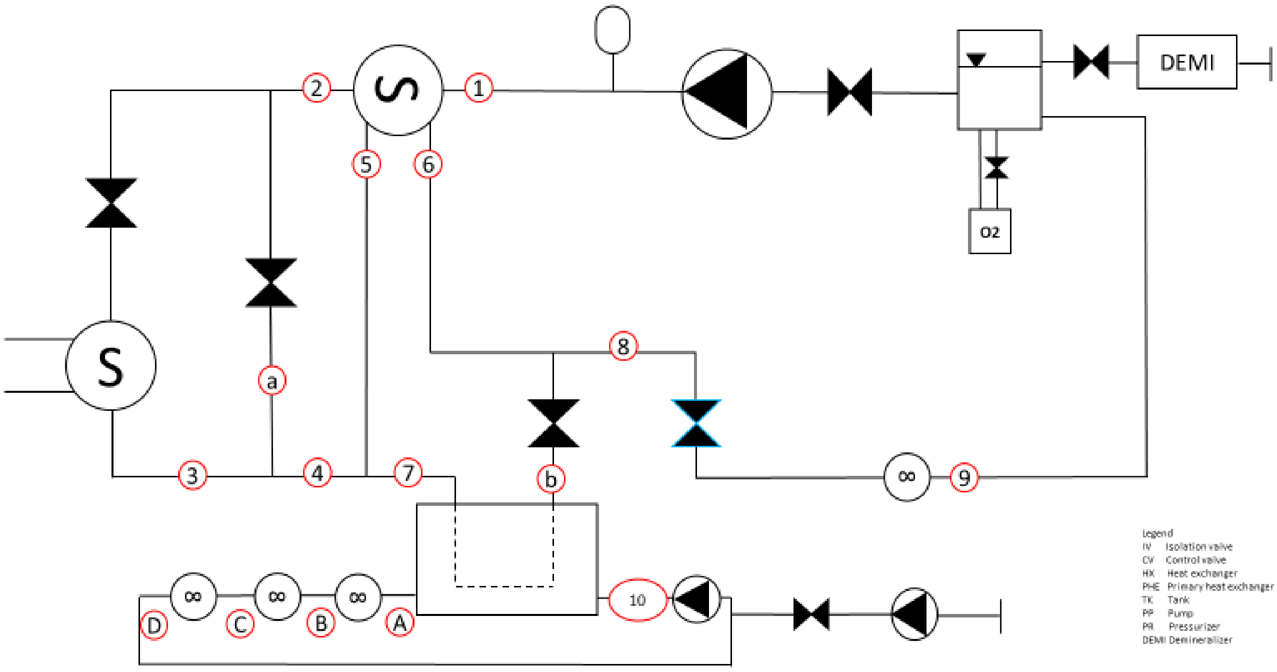

Fig. 5.8 – Design 4

Table 5.4 – Cycle temperatures

Point	Location	p [bar]	T [°C]	m [kg/s]
1	HX-201 cold side ingress	300	30	0,474
2	HX-201 cold side exit	300	350	
3	PHE exit	300	480	0,361
a	Bypass CV-201	300	350	0,113
4	Fluxes from phe and bypass	300	430	0,474
5	HX-201 hot side ingress	300	430	0,314
6	HX-201 hot side exit	300	97	0,314
7	Serpentine ingress	300	430	0,16
b	Serpentine exit	300	90	0,16
8	Fluxes from hx and serpentine	300	94	0,474
9	post depr. Cooling	1	30	0,474
10	Tank ingress, external	5	30	2,5
A	Tank exit	5	68	2,5
B	1st air cooler exit	5	52	2,5
C	2nd air cooler exit	5	42	2,5
D	3rd air cooler exit	5	31	2,5

In Table 5.5 are summarized pros and cons of the design presented, while in Table 5.6 are shown the items that have to be purchase.

The dimension of the main item to remove or purchase are the following:

- Tank-202: 2,3x1,15x1,77 m
- Oil Heat exchanger: L ~ 1000 mm D ~ 20 mm
- Air cooler: 1315x1008x776 mm (or 300 m^2)

Table 5.5 – Pros and cons

	Pros	**Cons**
Design 1	• Elimination of tank 202 clutter	• 4+ air cooler (1315x1008x776 mm) • Loss of HX-201 bypass • Changing in start-up procedure and flexibility
Design 2	• Same flexibility and start-up procedure as the original	• 4 SCW-oil heat exchangers (L~1000mm D~20mm) • 4 air-cooler (1315x1008x776 mm)
Design 3	• Equal to the original design	• Pressurized tank
Design 4	• More flexibility • No need to pressurize the tank	

Table 5.6 – New items

	Items to purchase
Design 1	• 6x 40-120 kW heat exchangers
Design 2	• 8x ~100 kW heat exchangers
Design 3	• 1x 250 kW heat exchanger
Design 4	• 2x 110 kW heat exchangers

5.5 Solution adopted for closed cycle

The solution adopted is Design 4, due to its minor changes compared to the original design, the few components to purchase and its simplicity compared to other design studied.

The numbers of air coolers needed comes from Excel calculations, but a preliminary RELAP5 simulation suggests 2 coolers of 39 m^2 each on the post-depressurization branch, instead of one, and 3 of 300 m^2 for the tank side, re-using the previous coolers of the open cycle. The final concept is shown in Figure 5.9. An expansions vessel is required: by calculating the volume, with formulas from (5.77) to (5.79), that water occupies when the system is cold and at 600 °C.

$$V(300\,bar; 20\,°C) = 44\,l = 0{,}044\,m^3 \tag{5.77}$$

$$V = \frac{m}{\rho\,(300\,bar; 600\,°C)} = 0.5036\,m^3 = 504\,l \tag{5.78}$$

$$\Delta = 504 - 44 = 460\,l\ =\ 0{,}46\,m^3 \tag{5.79}$$

Assuming 3 m height of water, an inner diameter of 0,442 m is obtained. Considering the pressurizing gas space, the total height of the expansion vessel is 5 meters.

The entire secondary system is then reduced in occupied volume, moving the CV-201 and IV-202 down. This branch is set parallel to the others pipes hosting valves, reconnecting it to the system, while the Tank-202 is shifted near the CV-203 and CV-205, shortening the relative piping.

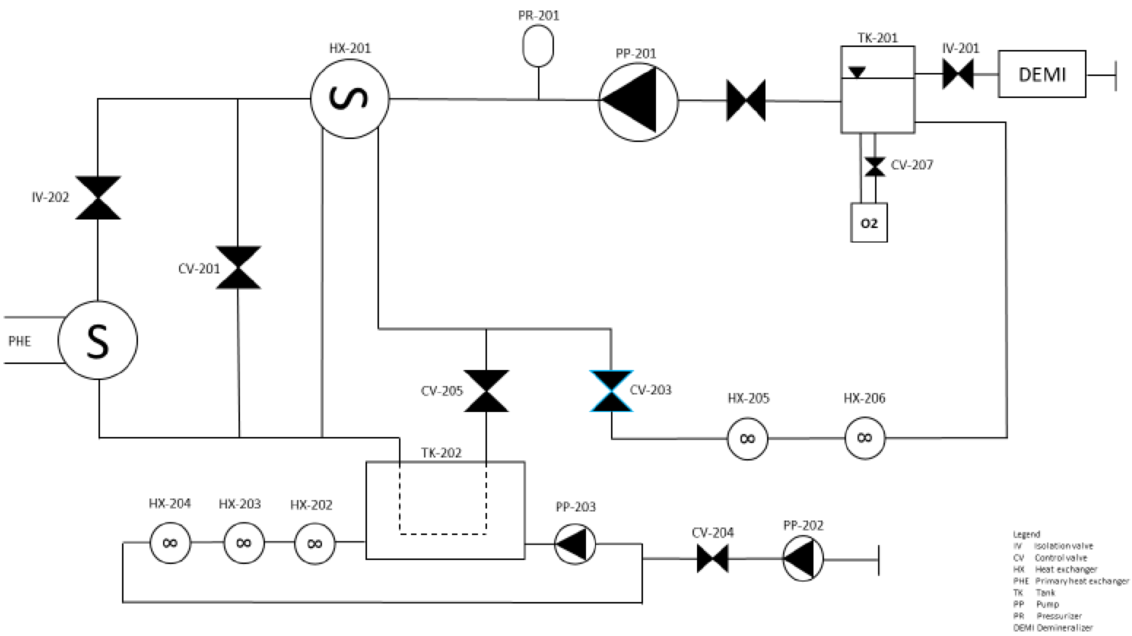

Fig. 5.8 – Final concept design

6. Thermal-hydraulic transient analysis

6.1 RELAP5 steady state results

A first simulation was conducted by closing the secondary loop, leaving the primary side pipes and most of the secondary in place. Only the air coolers were added.
The initialization of the closed secondary loop begun defining each component inlet mass flows, temperatures and pressures through corresponding inlet time-dependent-junctions and time-dependent-volumes. Several control variables were set to evaluate HX-201, PHE, serpentine and air coolers power exchanged.
The calculation time was set to 5000 seconds with minimum time steps of 10^{-8} s. The initial transient lasts 750 seconds, reaching then a steady state. This stability can be seen by the flat trend of the inlet and outlet temperature of the several heat exchangers.
After this first process analysis, the entire secondary loop was reduced in volume occupation, shortening the piping between the HX-201, CV-203, CV-205 and TK-202 and moving the CV-201 and IV-202 downward near the other two control valves. After this re-organization, a second simulation was conducted, with a total simulation time of 5000 and minimum time steps of 10^{-9} s. In Figure 6.1 the regenerative heat exchanger temperatures results are reported: after an initial transient and a brief adjustment after 1000 seconds, stability is reached. With an inlet cold side temperature of 30 °C, water exit the HX-201 at 364 °C, and from 438 °C is then cooled down on its hot side to 76 °C.
In Figure 6.2 Primary Heat Exchanger temperatures are shown: water is heated from 364 °C up to 520 °C, while lead is cooled from 538 °C to 398 °C.
In Figure 6.3 inlet and outlet serpentine temperatures reach stability at 438 °C and 112 °C respectively.
Mass flow rates of main branches can be seen in Figure 6.4: during stationary regime HX-201 cold side sees a flow rate of 0,474 kg/s. A mass flow of 0,339 kg/s passes through to the PHE, and a fraction of 0,168 kg/s goes into the serpentine, while the difference of 0,306 kg/s on the hot side of the HX-201. The same mass flow of 0,474 kg/s of the inlet passes through the depressurization valve.
Figure 6.5 and Figure 6.6 indicate exchanged powers of main heat exchangers and the ultimate outer air coolers. PHE has a regime power of 495 kW, while HX-201 of 738 kW. Instead, air coolers have a cooling power of 189,3 kW, 116,0 kW and 71,4 kW.

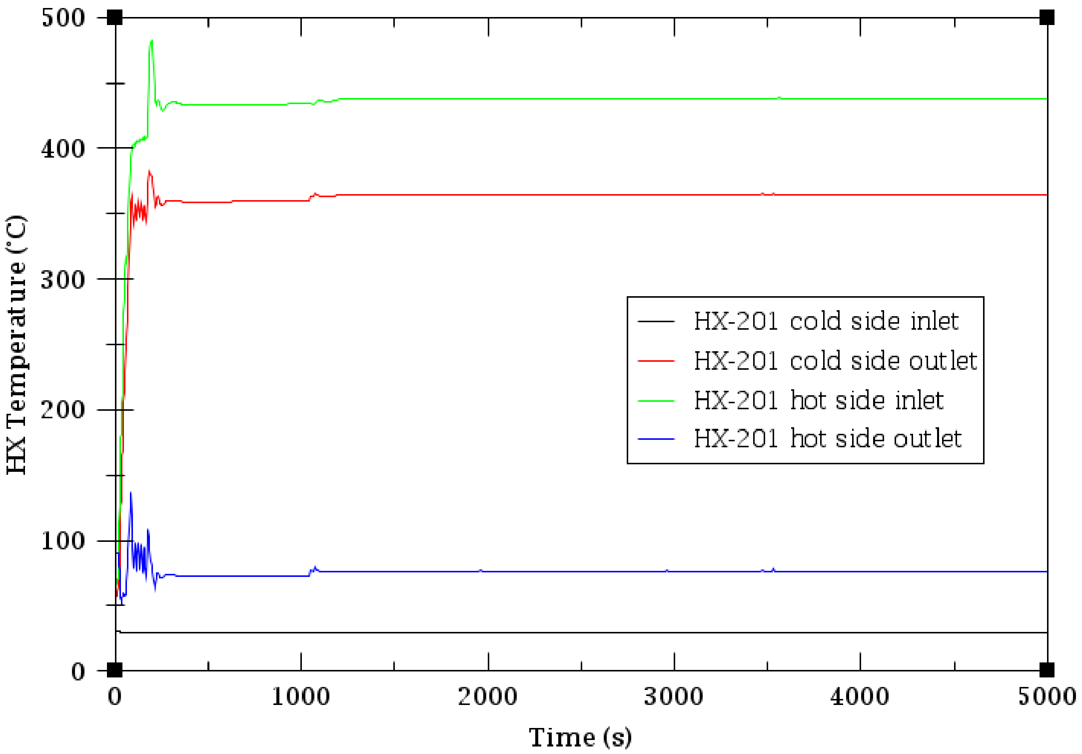

Fig. 6.1 - HX-201temperatures

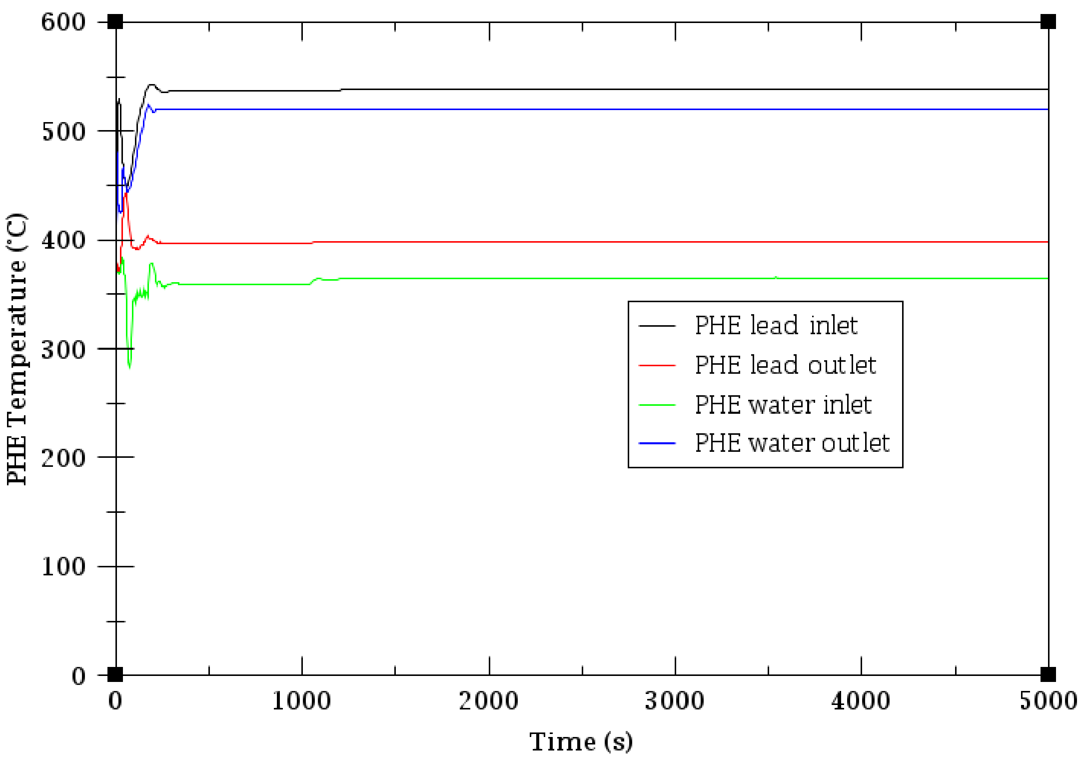

Fig. 6.2 - PHE temperatures

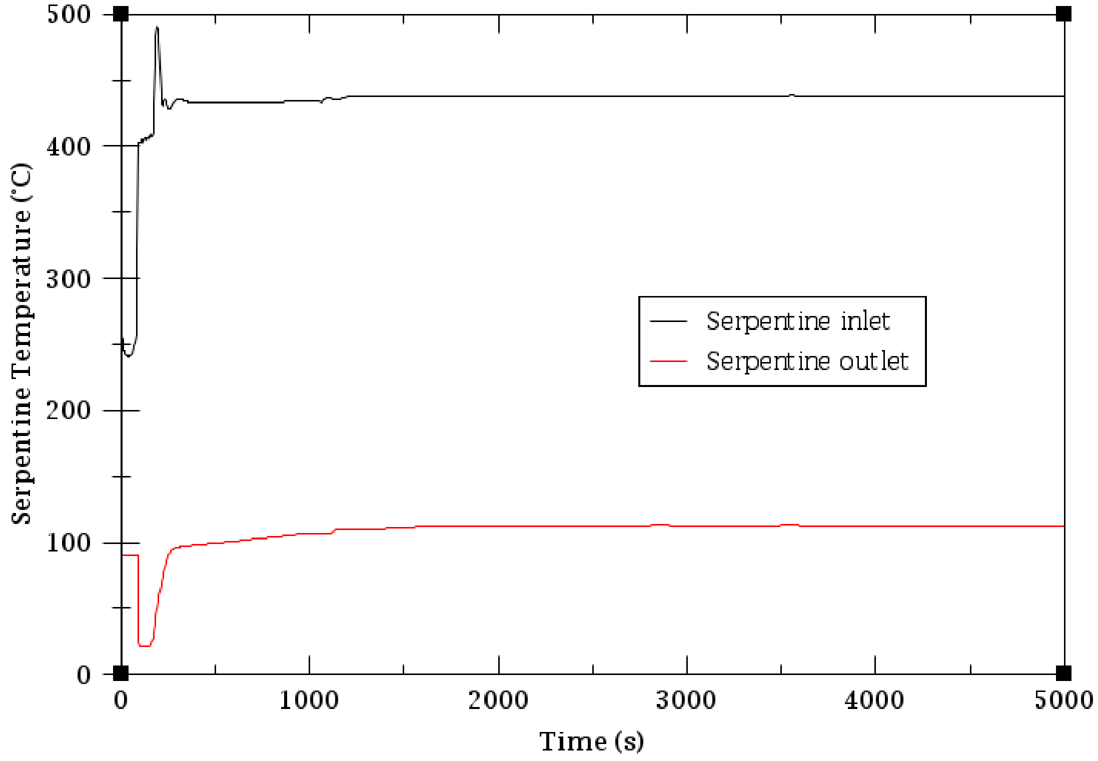

Fig. 6.3 - Serpentine temperatures

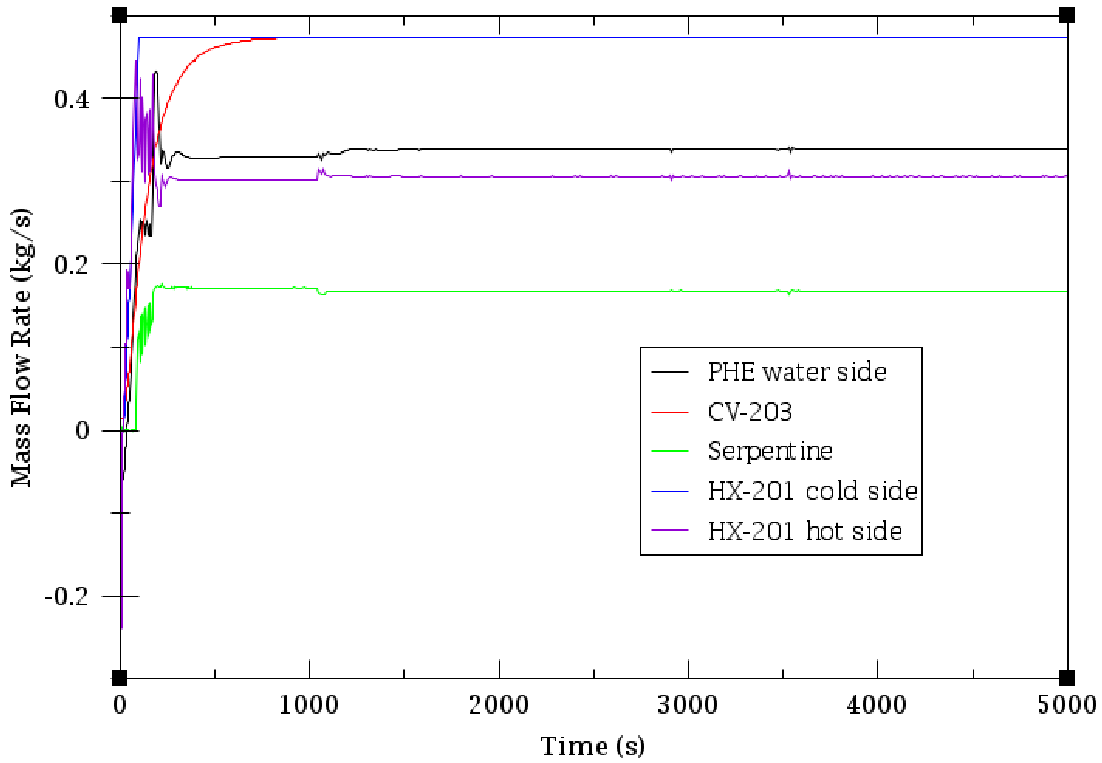

Fig. 6.4 - Mass flows

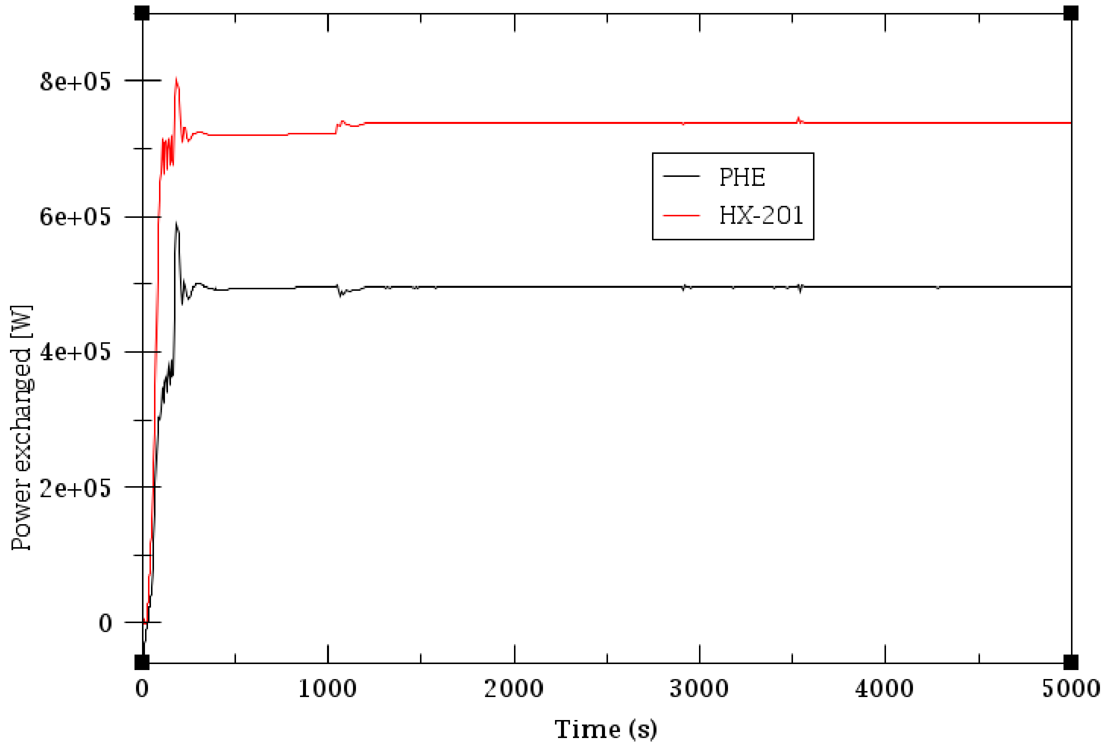

Fig. 6.5 – Heat Exchangers powers

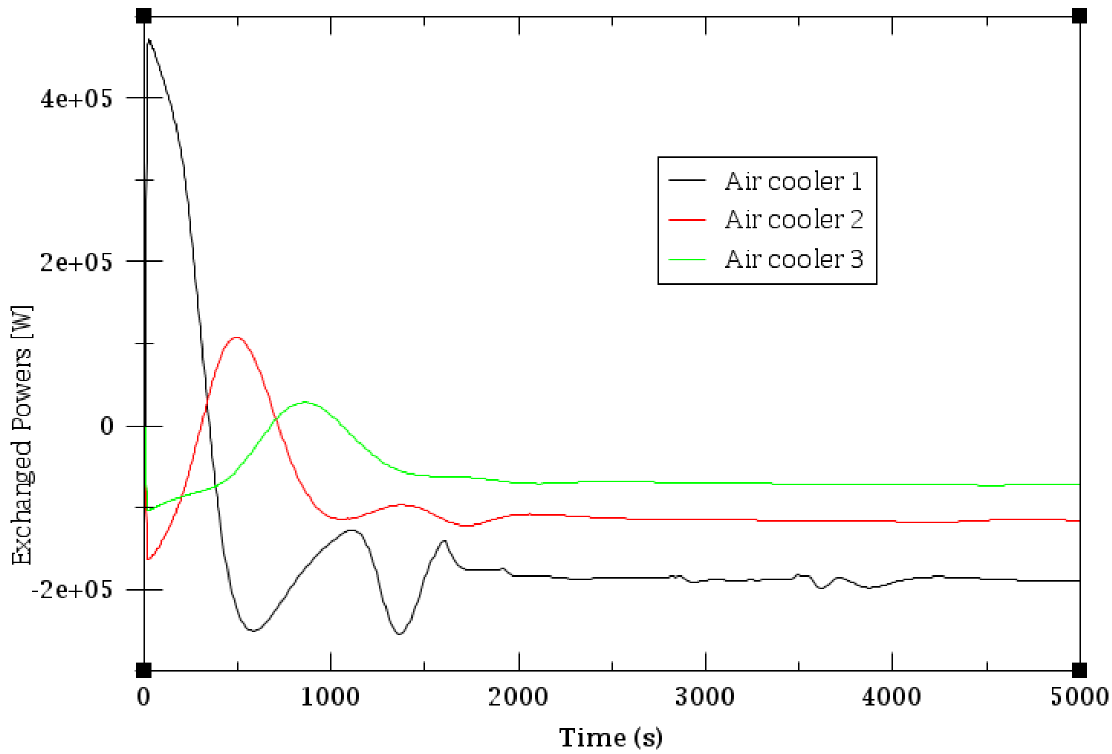

Fig. 6.6 – Condenser Air-Cooler powers

Comparison between numerical results and reference values is reported in Table 6.1, with percentual difference.

Table 6.1 – Differences between open and closed cycles

Parameter	Unit	Open cycle	Closed cycle	% Difference
HX-201 cold side inlet temperature	°C	20	30	50
HX-201 cold side outlet temperature	°C	350	364	4,0
PHE water side inlet temperature	°C	350	364	4,0
PHE water side outlet temperature	°C	520	520	/
HX-201 hot side inlet temperature	°C	430	438	1,86
HX-201 hot side outlet temperature	°C	90	76	-15,6
PHE lead side inlet temperature	°C	530	538	1,51
PHE lead side outlet temperature	°C	390	398	2,05
Serpentine inlet temperature	°C	430	438	1,86
Serpentine outlet temperature	°C	90	112	24,4
Temperature before CV-203	°C	90	89	-1,11
HX-201 power	kW	710	738	3,94
PHE power	kW	500	495	-1,0
Serpentine power	kW	~400	380	-5,0

In Table 6.2 exit temperatures and relative dissipated powers of the five air coolers are presented.

Table 6.2 – Air coolers values

	Exit temperature [°C]	Exchanged Power [kW]
Air Cooler depressurized water 1	44	84,6
Air Cooler depressurized water 2	29	30,9
Air Cooler tank side 1	49	189,3
Air Cooler tank side 2	38	116,0
Air Cooler tank side 3	30	71,4

6.2 Transient analysis

An accidental scenario has been analyzed to see the VLF closed cycle behavior during transient conditions. The “unprotected” loss of heat sink has been chosen: this consists in the recirculating pump loss due to a damage, stopping the Tank-202 outer water ring to be cooled down by air coolers and reducing its heat removal capability, leading a higher serpentine temperature exit. The secondary temperature transient is been evaluated.
The simulation is set in RELAP5 with a *restart* problem, continuing from the steady state and setting to zero the PP-203 time-dependent-junction mass flow. Simulation was conducted from 5000 to 10000 seconds, with a minimum time steps of 10^{-7}. The vertical light blue line in following graphs set the division when the transient begins.
In Figure 6.7 temperatures changes at serpentine inlet and outlet and before the depressurization valve are reported. It can be seen that, as expected, serpentine water temperature after 500 seconds suddenly rises, reaching a value of 402 °C at 8000 s and 410 °C at 10000 s, while temperature before CV-203 becomes 236 °C at 10000 seconds.
Valves adjust their position as in Figure 6.8: CV-201 begin to close, allowing more flow passing in the PHE, Figure 6.9, while CV-203 slightly opens. IV-201 and CV-205 remains totally open. Part of the fluid is redirected in the regenerative exchanger and not in the condenser.
As expected, the serpentine power exchanged drops, and at 8000 s is 100 kW (-73%) and at 10000 s is 76 kW (-80%), as shown in Figure 6.10.
A particular attention was given at the post-depressurization pressure value. Pressure rises, Figure 6.11, because control valve 203 tries to keep water in liquid phase, but Figure 6.12 demonstrates that fluid density drops after the valve, resulting in vapor production. Figure 6.13 shows that vapor generation begins after 571 seconds after transient occurs. So, after an accident happens and the ultimate heat sink pump is lost, operators have 9 minutes and 30 seconds to intervene and restore serpentine cooling, assuring a safe depressurization.

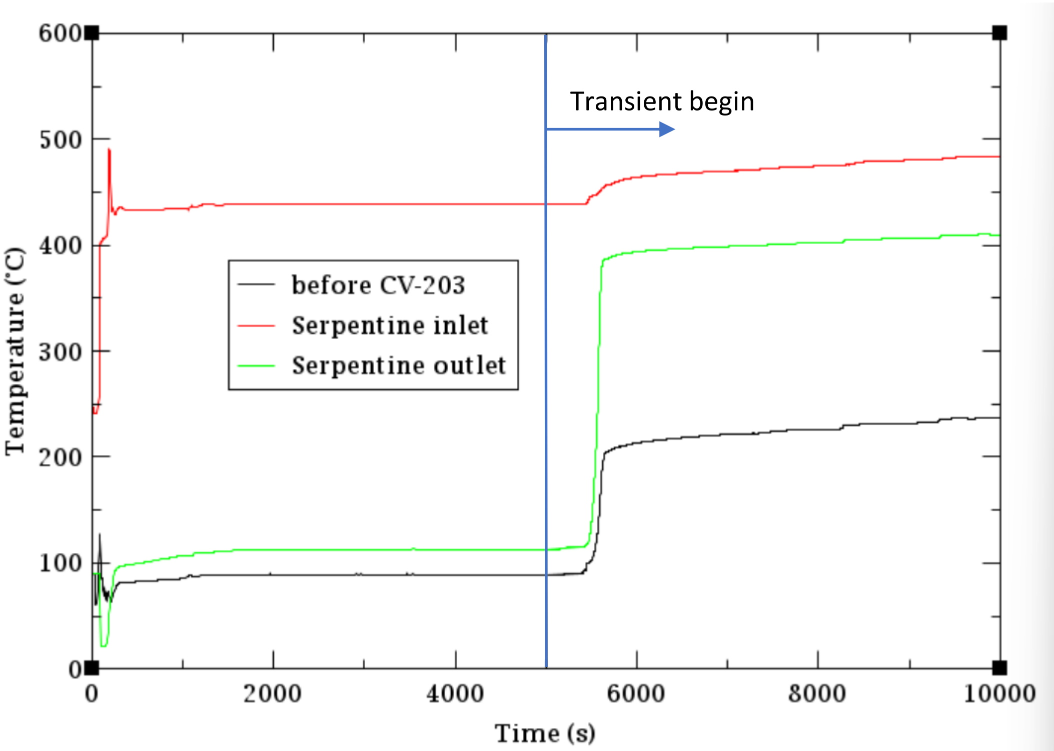

Fig. 6.7 – Inlet and outlet Serpentine Temperatures and pre-CV-203 Temperatures

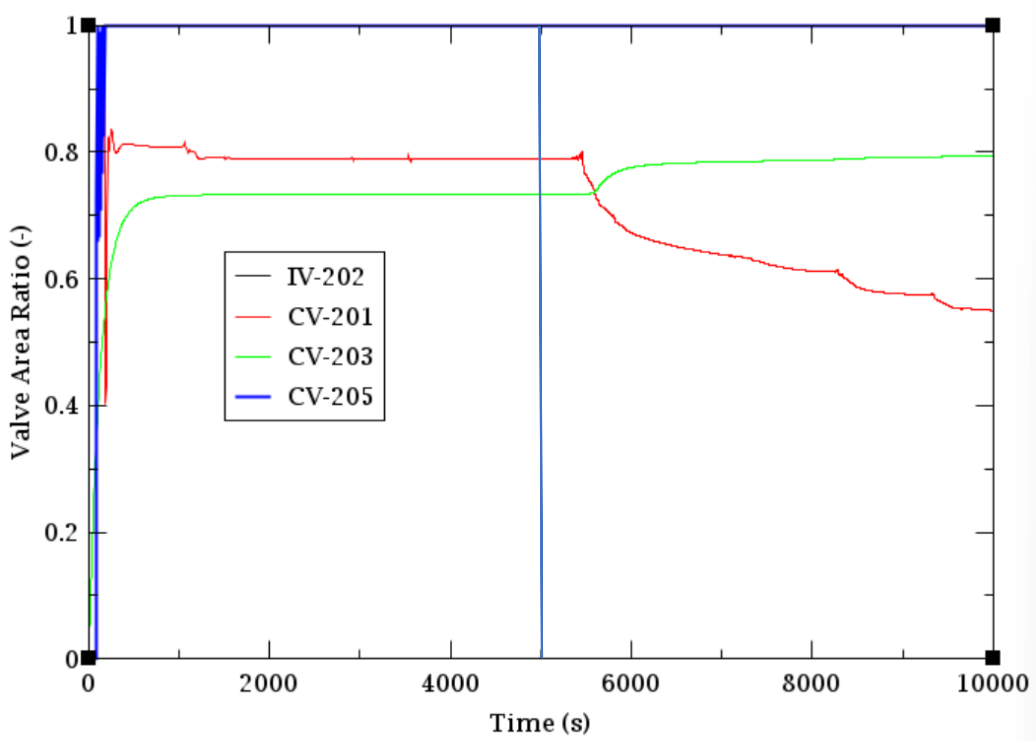

Fig. 6.8 – Valve area ratio

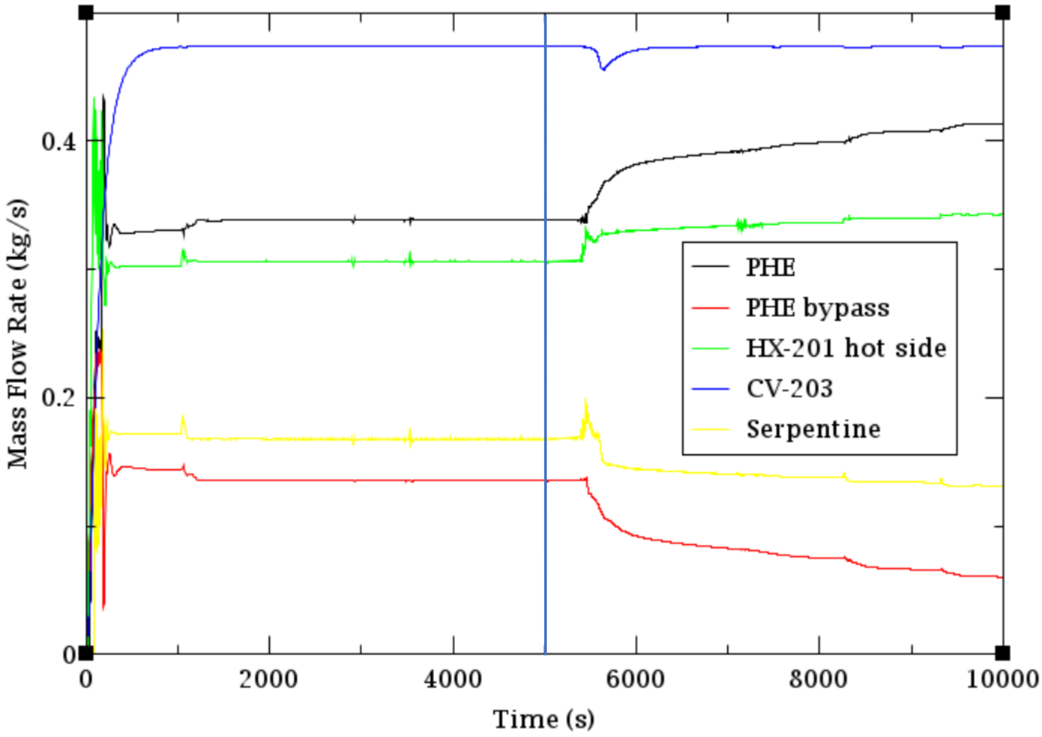

Fig. 6.9 – Heat exchangers mass flow rates

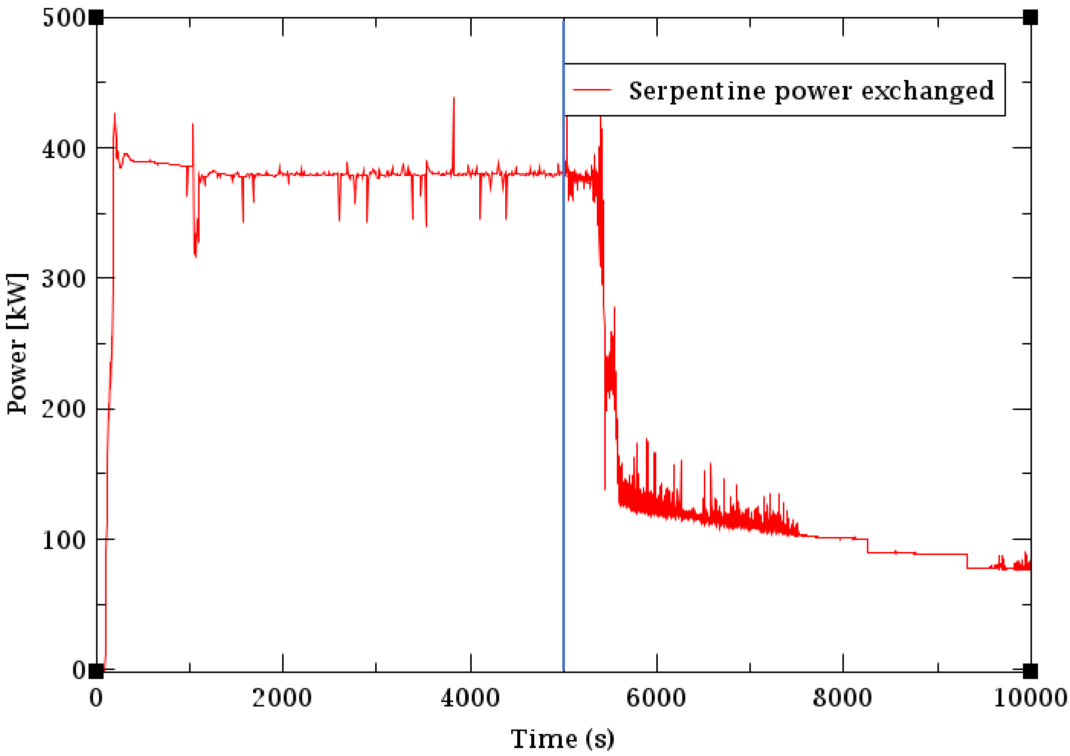

Fig. 6.10 – Serpentine Exchanged power

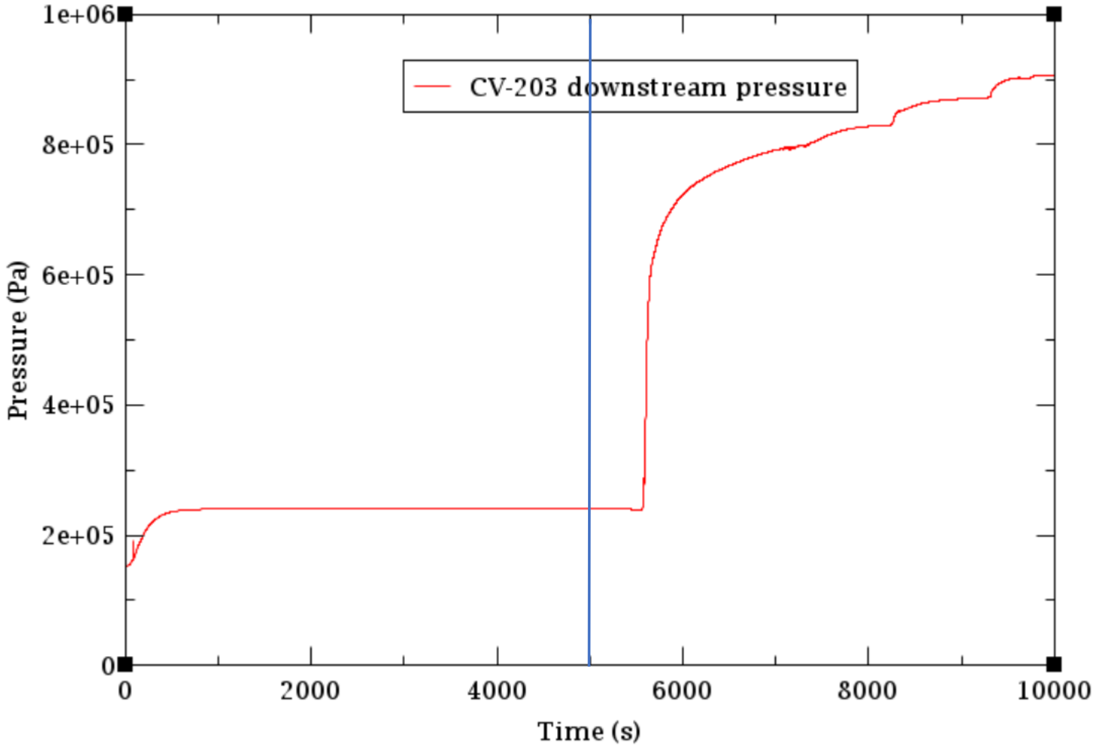

Fig. 6.11 – Pressure value downstream depressurization valve

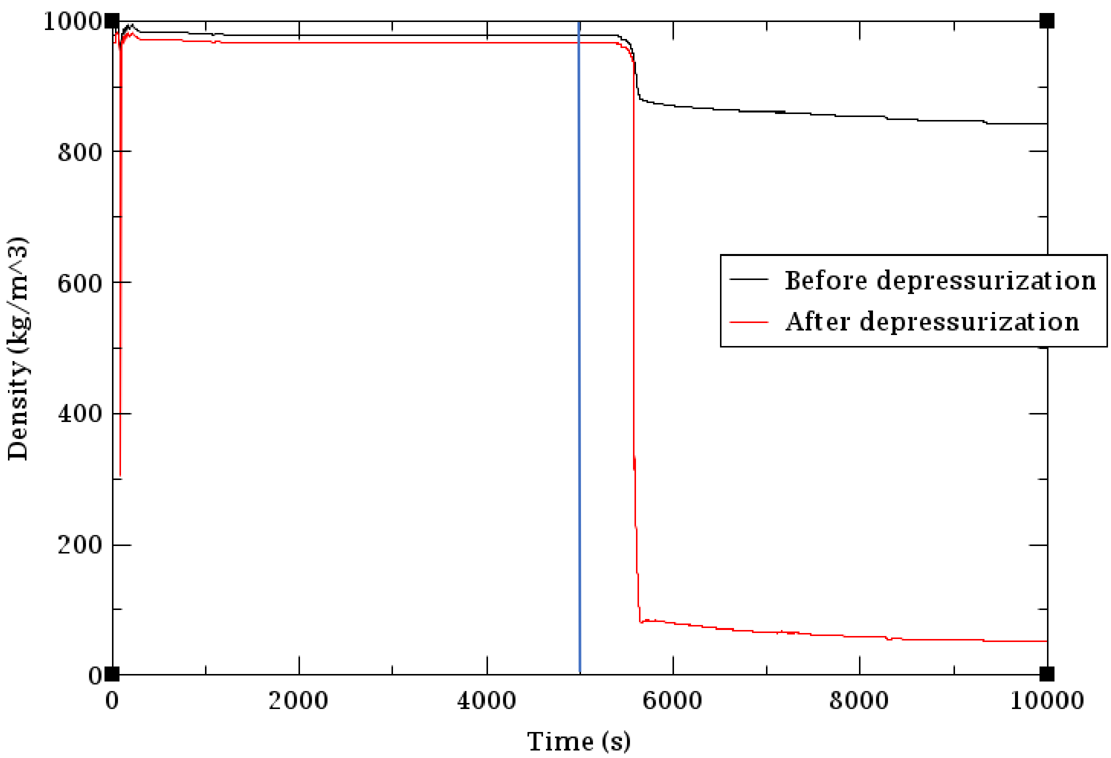

Fig. 6.12 – Density values before and after depressurization valve

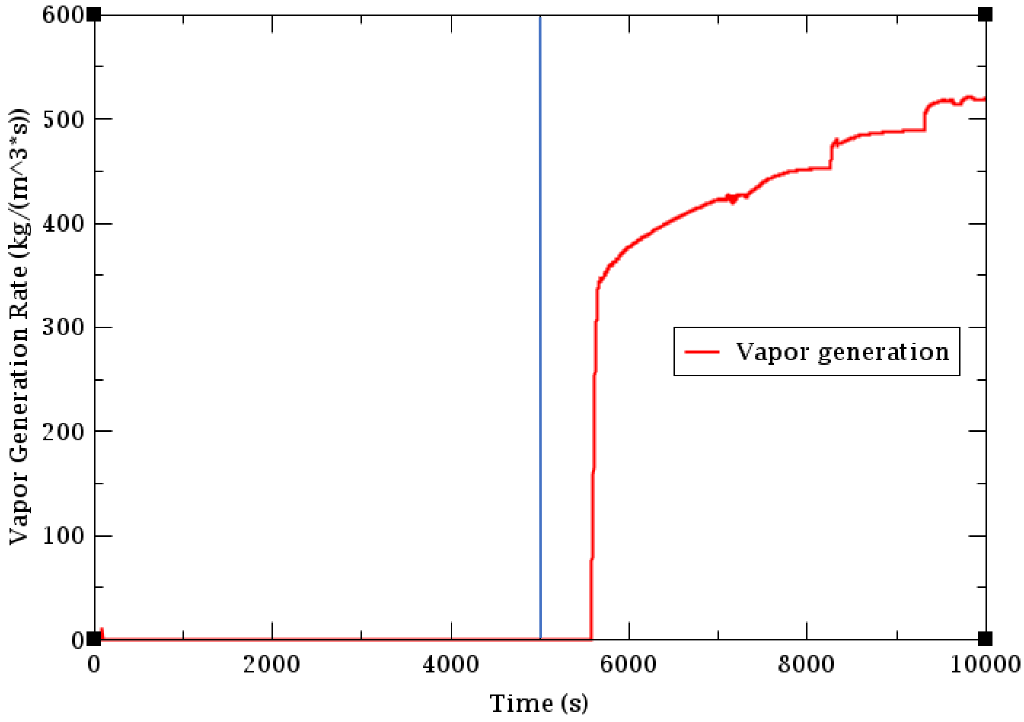

Fig. 6.13 – Vapor generation

7. Conclusions

In the present thesis designing and modeling of a closed-loop supercritical cycle for the Versatile Loop Facility was presented. The closure is reached dividing the system into two different rings: one is the depressurized water branch, cooled with air and sent back to a tank where the triplex pump takes feed water, and the second ring where shell-side water of condenser is cooled again with air and then recirculated in TK-202. Additional items to purchase are one air cooler of 300 m^2 (additional to the old ones) and two of 39 m^2. A chemistry control system and a pressurizer are also required. RELAP5 simulation shows the circuit is stable.
The transient analysis conducted shows that if the outer condenser cooling ring is lost due to accident, at depressurization valve water becomes steam into 9 minutes and 31 second, so measures must be taken before this time to assure a safe depressurization.

References

[1] T. R. Allen and D. C. Crawford, “Lead-Cooled Fast Reactor Systems and the Fuels and Materials Challenges” Science and Technology of Nuclear Installations, 2007

[2] IAEA-TECDOC-1746, Heat Transfer Behaviour and Thermohydraulics Code Testing for Supercritical Water-Cooled Reactors (SCWRs), Vienna (2014).

[3] PIORO, I. L., “Specifics of thermophysical properties and heat transfer at supercritical pressures in power-engineering applications: a review”, Proc. 12th Int. Symp. On Supercritical Fluids, Antibes Juan-Les-Pins, France (2018).

[4] KISS, A., Thermal Hydraulic Investigations of the Coolant Flow in Supercritical Water-cooled Reactor Relevant Geometries, Budapest University of Technology & Economics, Ph.D. Dissertation, (2018).

[5] CHENG, X., SCHULENBERG, T., Heat Transfer at Supercritical Pressures—Literature Review and Application to an HPLWR, Wissenschaftliche Berichte (Tech. Report) FZKA 6609, Forschungszentrum Karlsruhe, Mai (2001).

[6] MCADAMS, W.H., Heat Transmission, 2nd edition, McGraw-Hill, New York, (1942).

[7] MIHEJEV, M.A., Fundamentals of the Practical Calculations of Heat Transfer, 6th Hungarian Edition. Tankönyvkiadó, Budapest, (1987).

[8] PIORO, I.L., DUFFEY, R.B., Experimental Heat Transfer in Supercritical Water Flowing inside Channels (Survey), Nucl. Eng. Des., 235, 22, (2005), 2407–2430.

[9] PIORO, I.L., DUFFEY, R.B., Heat Transfer and Hydraulic Resistance at Supercritical Pressures in Power Engineering Applications, ASME Press (2007).

[10] FARAH, A., HARVEL, G., PIORO, I., Analysis of computational fluid dynamics code FLUENT capabilities for supercritical water heat-transfer applications in vertical bare tubes, ASME Journal of Nuclear Engineering and Radiation Science 2 (2016).

[11] JACKSON, J.D., HALL, W.B., Influence of Buoyancy on Heat Transfer to Fluids Flowing in Vertical Tubes under Turbulent Conditions, Hemisphere Publishing Company, Turbulent Forced Convection in Channels and Bundles, 2, (1979), 613–640.

[12] JACKSON, J.D., Consideration of the Heat Transfer Properties of Supercritical Pressure Water in Connection with the Cooling of Advanced Nuclear Reactors, Proc. 13th Pacific Basin Nuclear Conference, Shenzhen, 2002.

[13] ACKERMAN, J.W., Pseudo-boiling heat transfer to supercritical pressure water in smooth and ribbed tubes, J Heat Transfer, Trans. ASME, 92 3 (1970), 490–498.

[14] MOKRY, S., PIORO, I.L., FARAH, A., KING, K., GUPTA, S., PEIMAN, W.,

KIRILLOV, P.L., Development of Supercritical Water Heat-Transfer Correlation for Vertical Bare Tubes, Nuclear Engineering and Design, 241, (2011), 1126–1136.

[15] DYADYAKIN, B.V., POPOV, A.S., Heat Transfer and Thermal Resistance of Tight Seven-Rod Bundle Cooled with Water Flow at Supercritical Pressures, Transactions of VTI, 11, (1977), 244–253, (In Russian).

[16] PALKO, D., ANGLART, H., Investigation of the Onset of Heat Transfer Deterioration to Supercritical Water, Proc. 4th International Symposium on SCWRs, Heidelberg, 2009.

[17] BISHOP, A.A., SANDBERG, L.O., TONG, L.S., Forced Convection Heat Transfer to Water at Near-Critical Temperature and Supercritical Pressures, Westinghouse Electric Corporation Report (WCAP-2056), Pittsburg, 1964.

[18] AMBROSINI, W., FORGIONE, N., BADIALI, S., JACKSON, J.D., SHARABI, M., Capabilities of Two-Equation Low-Reynolds Number Turbulence Models in Predicting Heat Transfer to Fluids at Supercritical Pressure, Proc. 15th International Topical Meeting on Nuclear Reactor Thermalhydraulics (NURETH-15), Pisa, 2013.

[19] SHIRALKAR, B.S., GRIFFITH P., The Deterioration in Heat Transfer to Fluids at Supercritical Pressure and High Heat Fluxes, Report No. DSR 70332-55, Department of Mechanical Engineering, Massachusetts Institute of Technology, Cambridge, MA, USA, 1968.

[20] JACKSON, J.D., HALL, W.B., FEWSTER, J., WATSON, A. AND WATTS, M.J., Review of heat transfer to supercritical pressure fluids', H.T.F.S. Design Report No. 34, A.E.R.E. Harwell, (1975).

[21] JACKSON, J.D., HALL, W.B., Forced convection heat transfer to fluids at supercritical pressure, Turbulent Forced Convection in Channels and Bundles (eds. S. Kakac and Spalding D.B., Hemisphere Publishing Corporation, USA), pp 563-611, 1979a (1979).

[22] KRASNOSHCHEKOV, E.A., PROTOPOPOV, V.S., Experimental study of heat exchange in carbon dioxide in the supercritical range at high temperature drops, Teplofizika Vysokikh Temperatur, 4(3) (1966).

[23] PETUKHOV, B.S., KIRRILLOV, V.V., Questions concerning heat transfer in turbulent flow of liquids in tubes, Tepleonergetika No. 4 (1958) 63–68.

[24] PIORO, I., DUFFEY, R., DUMOUCHEL, T., Hydraulic Resistance of Fluids Flowing in Channels at Supercritical Pressures (Survey), Nuclear Engineering and Design, 231 (2) (2004) 187–197.

[25] CHENG, L., RIBATSKI, G., THOME, J.R., Analysis of Supercritical CO2 Cooling in Macroand Micro-Channels, International Journal of Refrigeration, 31 (8) (2008) 1301–1316.

[26] COLEBROOK, C.F., Turbulent Flow in Pipes, with Particular Reference to Transition Region between Smooth and Rough Pipe Laws, Institution of Civil Engineers of London -- Journal, 12 (4) (1939) 393–422.
[27] WELANDER, P., 1967, On the Oscillatory Instability of a Differentially Heated Fluid Loop, *J. Fluid Mech.*, Vol. 29, part 1, (1967) 17–30.

[28] LEDINEGG, M., Instability during Natural and Forced Circulation, Die Warme, Vol. 16, (1938).

[29] VISWANATHAN, R., COLEMAN K., RAO, U., Materials for Ultra-Supercritical Coal-Fired Power Plant Boilers, Int. J. Pressure Vessels and Piping 83 11–12 (2006) 778,783.

[30] GU, G.P., ZHENG, W., GUZONAS, D., Corrosion Database for SCWR Development, Proc. 2nd Canada-China Joint Workshop on Supercritical Water-cooled Reactors (CCSC-2010) Toronto,
2010.

[31] GUZONAS, D., NOVOTNY, R., PENTTILÄ, S., TOIVONEN, A., ZHENG, W., Materials and Water Chemistry for Supercritical Water-cooled Reactors, Woodhead Publishing Series in Energy, (2018).

[32] Fossil Plant Cycle Chemistry Instrumentation and Control—State-of-Knowledge Assessment. EPRI, Palo Alto, CA: 2007. 1012209.

[33] Interim Guidance on Chemical Cleaning of Supercritical Units. EPRI, Palo Alto, CA: 2010. 1017476.

[34] McDONALD, M.H., HYLAND, B., HAMILTON, H., LEUNG, L.K.H., ONDER, N., PENCER, J., XU, R., Pre-Conceptual Fuel Design Concepts for the Canadian Super Critical Water-Cooled Reactor, Proc. 5th Int. Symp. SCWR (ISSCWR-5), Vancouver, 2011.

[35] David Dalton, (2021). Fast Reactors/Ansaldo Nuclear Wins Contract to Work On Westinghouse Project. NUCNET. https://www.nucnet.org/news/fast-reactors-4-5-2021

[36] Liao J., Ferroni P. et al, Development of phenomena identification and ranking table for Westinghouse lead fast reactor's safety (2021), Progress in Nuclear Energy, 131,103577.

[37] IAEA, Advances in Small Modular Reactor Technology Developments, Vienna, September 2018.

[38] M. Caramello, Progress report on VLF Design and Test Matrix (Detailed Design),2021, Ansaldo Nucleare, AMR2-500-A003-PRO.

[39] Marcello Principato, VLF secondary loop RELAP5 nodalization and characterization, December 2022, ENEA.